Design of a Low Cost Hydrostatic Bearing

by

Anthony Raymond Wong

Submitted to the Department of Mechanical Engineering
in partial fulfillment of the requirements for the degree of

Master of Science in Mechanical Engineering

at the

MASSACHUSETTS INSTITUTE OF TECHNOLOGY

June 2012

Author .....
Department of Mechanical Engineering
May 17, 2012

Certified by .....
Alexander Slocum
Pappalardo Professor of Mechanical Engineering
Thesis Supervisor

Accepted by .....
David E. Hardt
Chairman, Department Committee on Graduate Theses

Design of a Low Cost Hydrostatic Bearing

by

Anthony Raymond Wong

Submitted to the Department of Mechanical Engineering
on May 17, 2012, in partial fulfillment of the
requirements for the degree of
Master of Science in Mechanical Engineering

Abstract

This thesis presents the design and manufacturing method for a new surface self compensating hydrostatic bearing. A lumped resistance model was used to analyze the performance of the bearing and provide guidance on laying out the bearing features. One arrangement of bearing features was cut into a flat sheet of ultra high molecular weight polyethylene which was then formed into a cylindrical shape. The shaped plastic was adhered to an aluminum housing then connected to a pump. Experimental data shows that the lumped resistance model provides a good estimation of the bearing performance. After validating the analytical model, sensitivity studies were conducted to predict changes in the bearing performance due to manufacturing variances. The results of the model indicate the design is extremely robust.

Thesis Supervisor: Alexander Slocum
Title: Pappalardo Professor of Mechanical Engineering

Acknowledgments

I want to start by thanking my God, without whom none of this would be possible.

My father has been an inspiration to me. His stories about MIT made me think it was somewhere I should go. His constant encouragement made me think MIT was somwhere I could go. Though he has never studied mechanical engineering, this thesis is part of his academic legacy.

I don't think words can adequately express my gratitude for my loving wife, Emily. Thank you for letting me go on this great adventure.

I am also immensely grateful to my thesis advisor, Dr. Alex Slocum. His energy and creativity motivated me to push forward. He had confidence in me (and the bearing), when I didn't.

Also I want to thank my lab mates in PERG. Zac Trimble took time from finishing his thesis to help me get the first test rig built. Folkers Rojas picked up the CFD and struggled with the theory with me. Mark Belanger at Edgerton Shop and Josh Dittrich were critical resources in building the hardware.

Contents

List of Figures

List of Tables

List of Variables

Symbol	Description	Units
A_l	area of lands	m^2
A_r	area of recessed regions	m^2
c	heat capacity	$\frac{J}{kg \cdot K}$
D_b	bearing diameter	m
e	eccentricity	
$\bar{F}$	load carrying efficiency	
g	acceleration due to gravity	$\frac{m}{s^2}$
h	bearing gap	m
H_f	friction power	W
h_o	gap when shaft is centered	m
H_p	pumping power	W
h_r	recess depth	m
k	stiffness	$\frac{N}{m}$
$\bar{K}$	specific stiffness	
L	length (parallel to fluid flow)	m
L_b	bearing length	m

Symbol	Description	Units
$\vec{n}$	normal vector	
p	pressure	$\frac{N}{m^2}$
p_r	recess pressure	$\frac{N}{m^2}$
p_s	supply pressure	$\frac{N}{m^2}$
Q	flow rate	$\frac{m^3}{s}$
$\bar{Q}$	specific flow rate	
R	fluid resistance	$\frac{kg}{s}$
r_i	inner radius	m
r_o	outer radius	m
u	fluid velocity in the x direction	$\frac{m}{s}$
U	relative surface speed	$\frac{m}{s}$
w	width (perpendicular to fluid flow)	m
W	load	N
δ	shaft displacement	m
ΔT	temperature rise	$^\circ C$
ζ	resistance ratio	
θ	angle around the bearing	$^\circ$
μ	viscosity	$\frac{N \cdot s}{m^2}$
ρ	density	$\frac{kg}{m^3}$
ϕ	angle of partial annulus	$^\circ$
ψ	additional collector land angle	$^\circ$

Chapter 1

Introduction

1.1 Motivation

The purpose of this research is to develop a surface self compensating hydrostatic journal bearing manufactured from a flexible material in a flat state which is then wrapped into a cylindrical shape and bonded in place. Areas of particular interest are cost reduction from traditional hydrostatic bearing manufacturing and unique performance features that can only be leveraged from bearings manufactured by this method.

The immediate motivation for this research is for naval propeller shafts. One common way to support propeller shafts are hydrodynamic bearings. Hydrodynamic bearings have some negative aspects such as wear during slow speeds or changes in the shaft direction of rotation and ingestion of debris along with the ocean water used to create the fluid film. A hydrostatic bearing would alleviate these adverse effects, but generally are more expensive due to complex fluid routing, cost of additional pumps, susceptibility to fouling or plugging, and multiple precision operations required during manufacturing. This research seeks to mitigate these impediments.

Another challenge naval bearing design is that sometimes there is a flange on the end of the shaft. Dry docking to repair bearings can be expensive. In order to facilitate repair in water without removing the shaft, bearings that are less than a 180° arc are investigated to fit over the flange. Surface self compensated hydrostatic

bearings have usually been made as a full journal bearings and partial arc bearings have not been made before.

1.2 Background

Hydrostatic bearings appear in the literature as early as 1851 [1]. The basic idea of a hydrostatic bearing is to pressurize a fluid to produce a fluid film between two surfaces which move relative to each other. The fluid film thickness is larger than the surface roughness, so the two surfaces never contact during motion. Additionally, because of the external fluid pressurization, the supporting force is independent of surface speed. This insensitivity to relative surface speed differentiates a hydrostatic bearing from a hydrodynamic bearing. Hydrodynamic journal bearings rely on the shaft speed to generate the fluid film and forces to support the shaft.

In hydrostatic journal bearings, fluid routings connect load bearing features, or bearing pads, to a compensator that regulates the fluid flow to the bearing pads and ensures a pressure differential between opposed load bearing areas, so that the bearing will apply a force to counteract external loads applied to the shaft. A variety of compensation methods exist such as fixed compensation which utilizes a fixed fluid resistance device such as a capillary tube or orifice. Constant flow compensation can be achieved by using separate pumps for each bearing pad or special valves. This work is primarily focused on self compensation which uses the gap between the surfaces of the bearing and the shaft as a variable restrictor to control flow. Early discussion of self compensation was presented by Hoffer [2]. Self compensation has the advantage that no tuning is required like fixed compensation. Also self compensation is resistant to clogging compared to other methods that involve small fluid openings.

Another hydrostatic bearing development of note was invented by Wasson et al. [3] which involved placement of all fluid routings on the surface of the bearing or shaft. They called it "surface self compensation" and had the unique feature that since all the hydraulic logic and connections were on the surface, the motion of the shaft and fluid shear cleans the surface features and thus it is extremely resistant to clogging. In

typical hydrostatic bearings, complex fluid routings move fluid from a compensator to the opposed bearing pad. These routings increase complexity and increase the susceptibility of plugging and fouling. Kotilainen and Slocum [4] expanded upon Wasson's work by casting the surface features into the inner diameter of a bearing sleeve. Previously, Wasson had machined the features into the outer diameter of the shaft.

Chapter 2

Design

2.1 Theory

2.1.1 Fluid Resistance

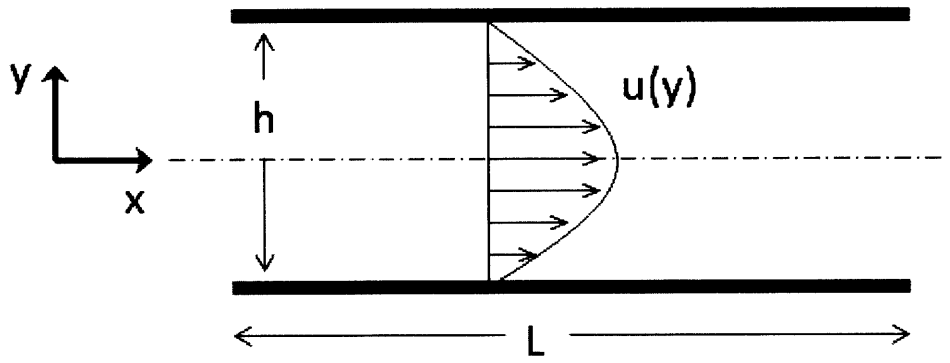

Figure 2-1: Parallel plate flow

To understand the theory behind hydrostatic operation, flow between two parallel plates of width, w, into the page as shown in Figure 2-1 caused by a pressure difference in the x-direction will be reviewed. The Navier-Stokes equation in the x-direction is as follows.

$$\rho g_x - \frac{\partial p}{\partial x} + \mu\left(\frac{\partial^2 u}{\partial x^2} + \frac{\partial^2 u}{\partial y^2} + \frac{\partial^2 u}{\partial z^2}\right) = \rho\frac{du}{dt} \tag{2.1}$$

Application of (2.1) requires the following conditions:

- A newtonian fluid which is true since this discussion is restricted to water
- Constant density which is true as long as temperature does not change significantly
- Constant viscosity which is also true as long as temperature does not change significantly

Assuming that the flow is fully developed, the flow, u, will be a function of y alone. Additionally, gravity effects will be considered negligible since the x-direction is perpendicular to gravity. Applying these assumptions simplifies (2.1) to the following.

$$-\frac{\partial p}{\partial x} + \mu \frac{\partial^2 u}{\partial y^2} = 0 \tag{2.2}$$

Solving (2.2) for the velocity yields the following.

$$u = \frac{1}{\mu}\frac{dp}{dx}\frac{y^2}{2} + C_1 y + C_2 \tag{2.3}$$

No-slip conditions exist at the interface of the fluid and the plates, so $u = 0$ at $y = \pm\frac{h}{2}$. Solving for the boundary conditions yields the equation for the fluid velocity profile.

$$u = \frac{1}{2\mu}\frac{dp}{dx}\left(y^2 - \frac{h^2}{4}\right) \tag{2.4}$$

Assuming a constant volume flow rate, the flow rate, Q, can be found by integrating the velocity profile as follows:

$$\begin{aligned} Q &= w\int_{-h/2}^{h/2} u(y)dy \\ &= -\frac{wh^3}{12\mu}\frac{dp}{dx} \end{aligned} \tag{2.5}$$

Solving for the differential pressure yields the following:

$$dp = -Q\frac{12\mu}{wh^3}dx \tag{2.6}$$

The negative sign in (2.6) indicates that the pressure decreases in the direction of the flow. At this point, an electrical circuit analogy is useful. Since the relationship in (2.6) between pressure and flow rate is not time dependent, this system acts like a resistor. This equation can be formed in a manner similar to Ohm's law, $V = IR$, where pressure serves the purpose of voltage and flow rate takes the place of current. Integrating (2.6) in x from 0 to L yields the following.

$$p = \frac{12\mu L}{wh^3}Q \tag{2.7}$$

(2.7) assumes that the outlet pressure is zero. From (2.7) it is easy to identify the resistance term. The fluid resistance of two parallel plates can described as the coefficients in front of Q. Mathmatically, the resistance is as follows.

$$R_{Parallel\ Plates} = \frac{12\mu L}{wh^3} \tag{2.8}$$

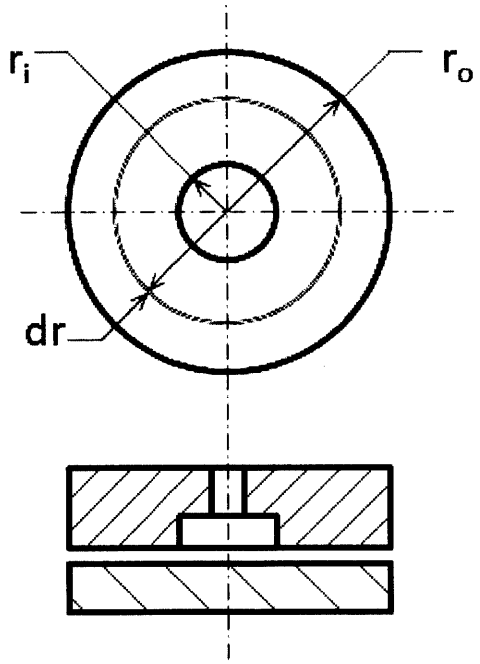

Figure 2-2: Flow through parallel annuli

Aside from parallel plates, the other geometric configuration that is common in hydrostatic bearings is two parallel annuli with flow going radially out from the center as shown in Figure 2-2. Analysis begins with an a thin ring of thickness dr. Because the thickness of the ring is small compared to the radius, the curvature is ignored and the parallel rings are modeled as two thin parallel plates of width, $2\pi r$, and length dr. Substituting these values into (2.6) yields the following.

$$dp = -\frac{12\mu Q}{2\pi h^3}\frac{dr}{r} \tag{2.9}$$

Integrating (2.9) from the inner radius of the annulus, r_i, to the outer radius, r_o, yields the following equation with the boundary condition of $p = 0$ at $r = r_o$:

$$p = -\frac{6\mu}{\pi h^3} ln\left(\frac{r_o}{r}\right) Q \tag{2.10}$$

At the inner radius of the annulus, the pressure is the same as the recess pressure.

$$p_r = -\frac{6\mu}{\pi h^3} ln\left(\frac{r_o}{r_i}\right) Q \tag{2.11}$$

Once again, using a circuit analogy gives the following equation for the fluid resistance.

$$R_{Annulus} = \frac{6\mu}{\pi h^3} ln\left(\frac{r_o}{r_i}\right) \tag{2.12}$$

For partial annular lands which are not a full circle as in Figure 2-3, (2.12) can be

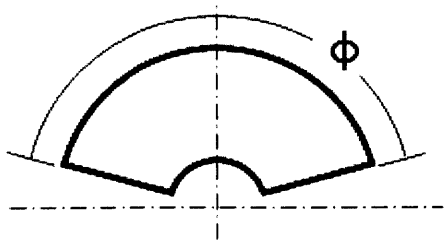

Figure 2-3: Partial annulus

modified to the following.

$$R_{Annulus} = \frac{6\mu}{\pi h^3} ln\left(\frac{r_o}{r_i}\right)\frac{360°}{\phi} \tag{2.13}$$

where ϕ is the angle that the circular land covers in degrees.

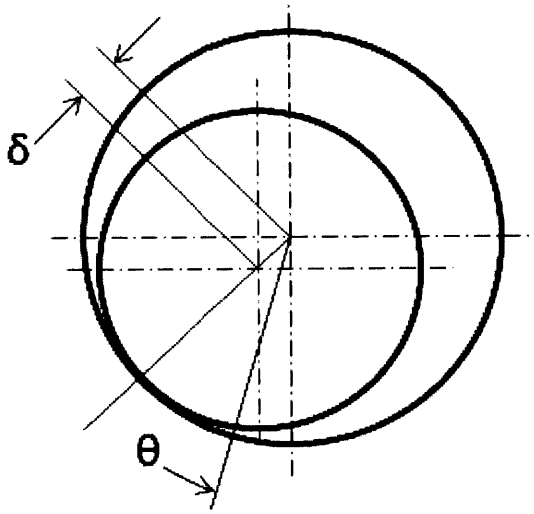

Figure 2-4: An eccentric shaft in a bearing

While these analyses for parallel surfaces are convenient from an analysis standpoint, in most cases of interest surfaces in a journal bearing are not parallel. If the shaft is not centered as shown in Figure 2-4, the gap is not constant. For a shaft that is not centered, the shaft eccentricity is defined as

$$e = \frac{\delta}{h_o} \tag{2.14}$$

In (2.14) h_o is the bearing gap at a reference position. For journal bearings, the reference position is when the shaft and bearing are concentric. δ is the distance between the axes of the shaft and bearing. The bearing gap, h, can then be described as a function of eccentricity and angle, where the angle is measured from the line

going through the centerlines of the bearing and shaft.

$$h = h_o[1 - e\cos(\theta)] \tag{2.15}$$

(2.15) could then be substituted into (2.6). However, Kotilainen [5] numerically shows that for hydrostatic journal bearing design approximating these surfaces as parallel plates is sufficient for calculating resistances and is accurate to within 4% when the feature circumferential width is less than 10% of the diameter.

2.1.2 Bearing Pad Load

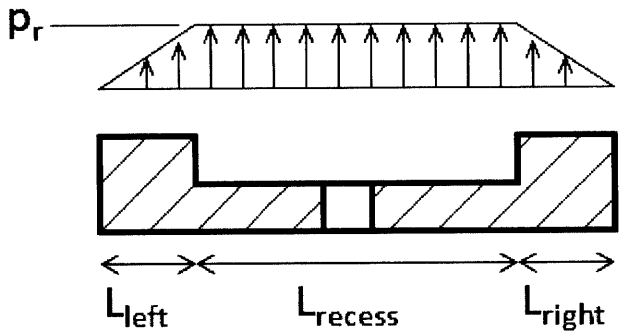

Figure 2-5: Rectangular pad with pressure profile

Hydrostatic bearings are usually comprised of load carrying areas called bearing pads. Bearing pads are recesses surrounded by raised lands. The pressure in the recess is considered constant due to its depth. This assumption arises from (2.6). When h is large, dp becomes small especially since the relationship is cubic. In the lands, the pressure decreases to the pressure outside the bearing pad, usually atmospheric pressure. The load from any fluid can be calculated by integrating the pressure:

$$\vec{W} = \int_A p\vec{n}dA \tag{2.16}$$

where $\vec{n}$ is the normal vector. For the example in a long rectangular bearing pad as in

Figure 2-5, the pressure decreases linearly in the lands. For this example, the bearing length into the page, w, is long such that flow out the ends is negligible. Determining the load of this bearing pad is easily accomplished by finding the volume of the triangular prisms on the left and right lands and the volume of the rectangular prism in the recess.

$$\begin{aligned} W &= W_{land\ left} + W_{recess} + W_{land\ right} \\ &= \frac{1}{2} w L_{left} p_r + w L_{recess} p_r + \frac{1}{2} w L_{right} p_r \end{aligned} \tag{2.17}$$

Similar analysis can be done for an annulus. Combining (2.10) and (2.11), an expression for the pressure distribution in the land region is derived:

$$p = \frac{p_r}{ln\left(\frac{r_o}{r_i}\right)} ln\left(\frac{r_o}{r}\right) \tag{2.18}$$

Substituting, (2.18) into (2.16) with the area defined as a strip of length $2\pi r$ and width dr yields the following:

$$\begin{aligned} W_{Annulus\ land} &= \int_{r_i}^{r_o} \frac{p_r}{ln\left(\frac{r_o}{r_i}\right)} ln\left(\frac{r_o}{r}\right) 2\pi r dr \\ W_{Annulus\ land} &= \frac{\pi p_r}{2ln\left(\frac{r_o}{r_i}\right)} \left(r_o^2 - r_i^2\right) - \pi p_r r_i^2 \end{aligned} \tag{2.19}$$

2.1.3 Fluid Resistance Network

To find the load bearing performance of a hydrostatic bearing, the system can be modeled as a fluid resistance network. The raised lands represent resistors while the deeper grooves represent nodes where the pressure is roughly equal for the purposes of the analysis. Once the system has been modeled as a resistance network, Kirchhoff's Current Law and Kirchhoff's Voltage Law can be employed to solve the network. The pressures at the nodes are then used to calculate the bearing load.

2.1.4 Dimensionless Parameters

To facilitate the comparison of various bearing designs, dimensionless parameters have been developed to measure performance. For this discussion, the performance measures used by Wasson [6] will be used. The first is the load carrying efficiency, which is expressed as follows:

$$\bar{F} = \frac{F_y}{p_s L_b D_b} \tag{2.20}$$

The load carrying efficiency normalizes the force the bearing exerts to support the shaft by the force that would result by applying the pressure supply on the projected area of the bearing. The bearing force is a function of the gap, so a standard gap distance needs to be chosen so the bearings can be compared fairly. The load carrying efficiency for this thesis will be measured at 75% gap closure, or $e = 0.75$. It should be noted though that 75% gap closure may be too close to failure for some bearing designs. More conservative designs or designs with looser tolerances on the bearing and shaft should consider calculating load carrying efficiencies at lower eccentricities, so realistic values that would be seen in operation are reported.

The second important dimensionless performance parameter is the specific stiffness. The specific stiffness is defined by Wasson as follows:

$$\bar{K} = \frac{\bar{F}}{e} \tag{2.21}$$

Obviously, specific stiffness is dependent on eccentricities, so specific stiffness is usually measured a low eccentricities of less than 0.01 to capture the initial specific stiffness. Partial arc bearings or any gravity preloaded bearing needs to be treated slightly differently because the net bearing force is not zero at zero eccentricity. For this work, the initial specific stiffness will be calculated as the change in load carrying efficiency divided by the change in eccentricity for a change in eccentricity from 0 to 0.01.

$$\bar{K}_o = \frac{\Delta \bar{F}}{\Delta e} \tag{2.22}$$

Flow rate is non-dimensionalized by dividing it by the flow that would occur if

the flow went through an annulus the same size as the clearance when the shaft is centered in the bearing. The formula for specific flow rate is as follows:

$$\bar{Q} = \frac{Q}{\left(\frac{p_s \pi D_b h_o^3}{12 \mu L_b}\right)} \tag{2.23}$$

Resistance ratio is another variable frequently used in the design of bearings. It is the ratio of the inlet fluid resistance across the compensator to the outlet resistance across the lands.

$$\zeta = \frac{R_{in}}{R_{out}} \tag{2.24}$$

2.1.5 Friction Loss and Temperature Rise

Because of friction losses due to shearing the fluid, hydrostatic bearings will cause a rise in temperature of the fluid. The friction power is the power needed to shear the fluid when two surfaces move relative to each other. It can be calculated by the following from [7].

$$H_f = \mu U^2 \left(\frac{A_l}{h} + \frac{4A_r}{h_r}\right) \tag{2.25}$$

Here U is the relative surface speed and for a journal bearing is a function of the angular velocity of the shaft. The two terms in (2.25) represent the power loss due to friction for the lands and recesses, respectively. The coefficient of four for the recess friction term is a correction for recirculation flow in the recess. The pumping power, or power needed to move the fluid through the bearing, is defined as the following:

$$H_p = p_s Q = \frac{p_s^2}{R} \tag{2.26}$$

These two power losses become the total power dissipated by the bearing, or

$$H_t = H_p + H_f \tag{2.27}$$

Both terms in (2.27) are related the bearing gap and can be written as follows.

$$H_t = C_1 h^3 + \frac{C_2}{h} \tag{2.28}$$

C_1 is a related to the land geometry and supply pressure. C_2 is related to the surface area of the bearing and surface speed of the shaft. It can immediately be seen that pumping losses increase with bearing gap while shear losses decrease with increasing gap.

The temperature rise can then be described as follows.

$$\begin{aligned} \Delta T &= \frac{H_t}{Qc\rho} \\ &= \frac{p_s}{c\rho}\left(1 + \frac{H_f}{H_p}\right) \end{aligned} \tag{2.29}$$

When the shaft is not rotating, the temperature rise in the fluid simplifies to the following.

$$\Delta T = \frac{p_s}{c\rho} \tag{2.30}$$

For water, which is the fluid of interest, at 20°C, the temperature rise (°C) due to supply pressure only is

$$\Delta T = 2.397X10^{-7} p_s \tag{2.31}$$

where p_s is the pump supply pressure in N/m^2.

2.2 General Design Guidelines

Given the previous discussion concerning the theory behind hydrostatic bearings, the design of such a bearing may appear intimidating. However, design of a hydrostatic bearing is actually fairly straight forward. Suppose a problem begins with a shaft of a certain diameter and load that needs to be supported.

1. Size a pump to see if it is feasible to support the load with a given pumping pressure. As a general rule of thumb the load carrying efficiency of a surface

self compensated bearing is 0.2-0.3. Using equation (2.20) the load that the bearing could support can be calculated.

2. The bearing gap should be determined. The performance with respect to pumping power is improved by reducing the bearing gap, while shear power is worse with decreasing gap. In later stages of design after the bearing features have been determined, the bearing should be optimized to reduce power losses by finding the minimum power from (2.28). To start though, DIN standard 31652 [8] provides the information in Table 2.1 for minimum film thickness for hydrodynamic bearings. These empirical recommendations assume peak to valley surface roughness of less than 4μm, minor geometrical errors, filtering of the fluid and running-in of the bearing. This table gives the lower bound of the bearing gap to prevent contact between the asperities on the shaft and bearing. Manufacturing limitations will prevent most designs from using such small bearing gaps. Another rule of thumb in hydrodynamic bearing design is to use a bearing radius to radial bearing gap ratio of 1000 [9]. For lack of better guidelines this rule of thumb will suffice as a starting point for hydrstatic bearing designs. Finally, one other consideration for bearing gap is the ratio of gap to groove depth. Usually the bearing gap will drive the groove depth and not the other way around, but for bearings cut into flat sheets the limits on the sheet thickness may cause issues. For the grooves to function as nodes they need to be significantly lower resistance than the raised lands. At a minimum the grooves should be 10 times deeper than the bearing gap. Ideally, they should be 15 times the bearing gap.

3. Determine the bearing length to diameter ratio based on the space available. The length should be at least as large as the diameter for pure radial support. If moment loads need to be supported, two bearings each of at least one shaft diameter in length should be about 3 shaft diameters apart center to center. This rule of thumb comes from Saint-Venant's principle.

4. Select the circumerferential angle the bearing will cover. Partial arc bearings

Table 2.1: Minimum film thickness in μm based on shaft surface speed

Shaft diameter (mm)		Sliding speed of shaft (m/s)				
Over		-	1	3	10	30
	Up to	1	3	10	30	-
24	63	3	4	5	7	10
63	160	4	5	7	9	12
160	400	6	7	9	11	14
400	1000	8	9	11	13	16
1000	2500	10	12	14	16	18

much less than 180° will have problems creating opposed differential pressure to recenter the shaft from perturbations. Also partial arc bearings have circumferential leak paths, so they will require more flow than a full journal bearing where fluid can only exit axially. Knowing the length, diameter and angle of coverage, a rectangular footprint available for the hydrostatic features can be determined.

2.2.1 Laying Out Hydrostatic Features

Now that the available area for the hydrostatic features is bounded, grooves need to be designed to route the fluid and make the surface self compensating bearing. There is great latitude in what could work. The following discussion attempts to provide some suggestions on how to start.

1. Start by placing the inlets. The radial position of the shaft will be sensed in the region around the inlets. The inlets should be distributed in such a way that the bearing is sensitive to shaft movement in directions needed for the design.

2. Separate the inlet port from a collector groove with a land region. This land will be the compensating resistor and control the flow to the bearing pad.

3. Place the load carrying areas nominally on the opposite side of the shaft. The positions of the load carrying areas and compensators are crucial, since the

compensator will sense the location of the shaft and the load carrying areas will apply the reaction force.

4. Connect the collector to the load carrying area with a groove.

5. Model the surface as a node network. Treat the recessed areas as nodes. Account for all the flow going out of the inlets and in and out of the nodes.

6. Divide the surface into logical sub regions for calculations. From the discussion in 2.1.1, keep the circumferential width of the sub regions less than 10% of the diameter, so a single gap value can be used for the sub region. Using circular and rectangular sub regions eases calculations. Divide up the lands into regions to calculate the resistances. Divide the load bearing pads into regions to calculate the forces.

7. Based on the dimensions of the region calculate fluid resistances between regions. Use the distances from the assumed direction of shaft movement to calculate the angle of the land. Calculate the bearing gaps by using (2.15).

8. Solve the node network for the pressures in the recesses.

9. Calculate forces from the bearing pads.

10. Adjust the geometry to achieve the desired performance.

See Appendix A for an example of how the surface of a bearing was discretized into lumped resistances and analyzed to determine performance.

2.3 Design

The initial concept for the partial arc bearing included two pockets as shown in Figure 2-6a. In these concept sketches the circular areas represent the inlet and compensator. The rectangles represent the bearing pad areas. In the first concept, the center of the bearing pads are offset axially and would allow a twisting moment on the shaft. Figure 2-6b shows a second concept that removes the twisting moment at the expense

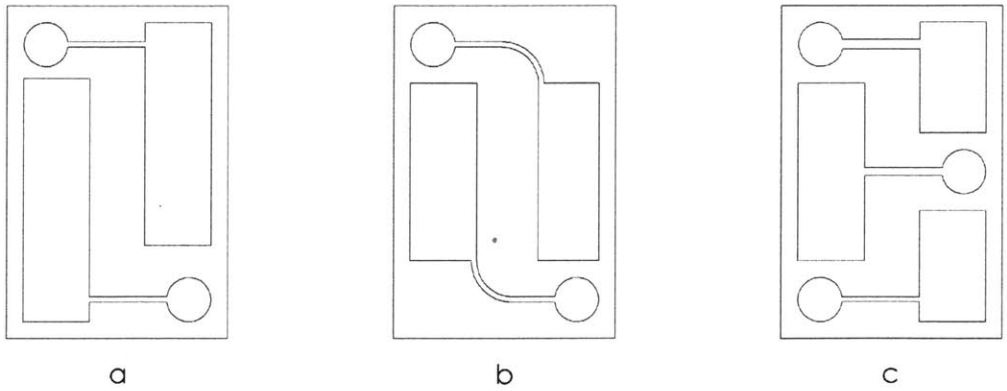

Figure 2-6: Sketches of the progression of bearing concepts

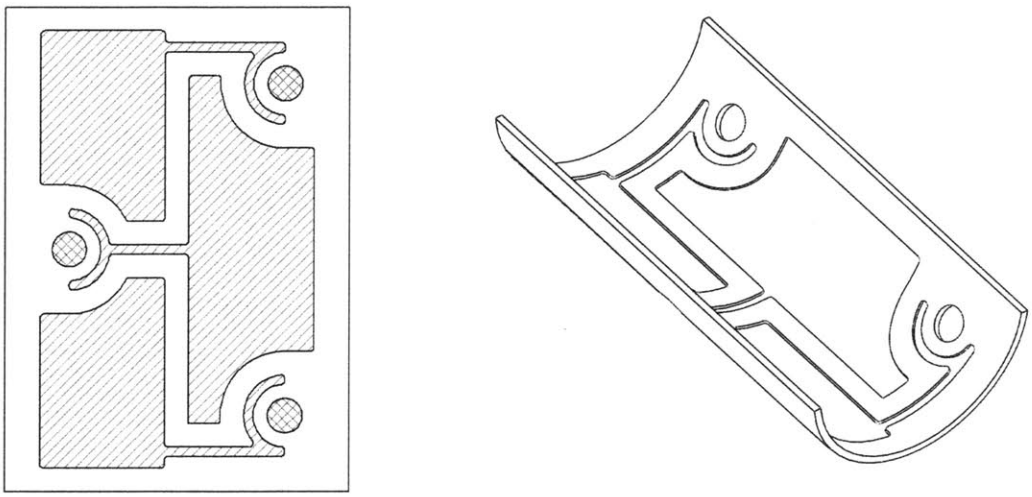

Figure 2-7: Model of pattern cut into flexible material

of bearing pad area. If the bearing pads are thought of as point loads, the shaft is supported by only two points. No matter how arranged, two support points are not stable and a second bearing would be required. In the final concept a third pocket was added to provide tilt stiffness and resist twist shown in Figure 2-6c. The bearing features were designed to be machined into a flat flexible material and adhered to half of a cylinder. The pattern for the test bearing is shown in the left side of Figure 2-7. The cross-hatched circular regions are the inlets. The hatched regions are the recessed areas while the white areas are the raised lands. A rendering of the bearing formed into a cylinder is shown on the right side of Figure 2-7. Sensitivity studies

examining the amount of collector wrap and collector land thickness are discussed in section 3.2.1. The bearing covers 165° of the the shaft and was designed for a nominal bearing gap of 127 μm for a shaft diameter of 100 mm. The groove depth was selected to be 10 times deeper than the bearing gap. Since the resistance is inversely proportional to the gap cubed, the resistance in the grooves would be 1000 times less than the raised areas. This low resistance allows the grooves to be treated as constant pressure nodes.

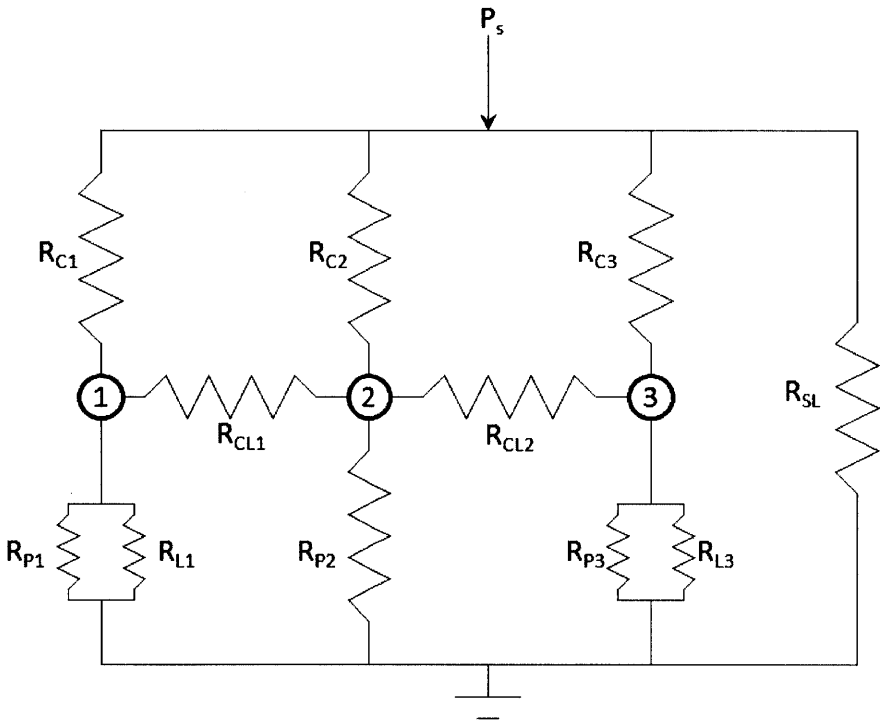

Figure 2-8: Resistance network model

Based on the previously discussed theory, the bearing surface is modeled as a resistance node network shown in Figure 2-8. The subscript 'C' indicates that the resistance is for the compensator, 'CL' for cross leakage between nodes, 'P' for leakage out of the load bearing pad, 'L' for leakage, and 'SL' for supply leakage directly from the inlet to the bearing outlet. Figure 2-9 shows how the topology of the bearing was turned into resistances. The hatched regions are numbered and indicate the nodes or constant pressure regions. Further discussion of how the topology was lumped into

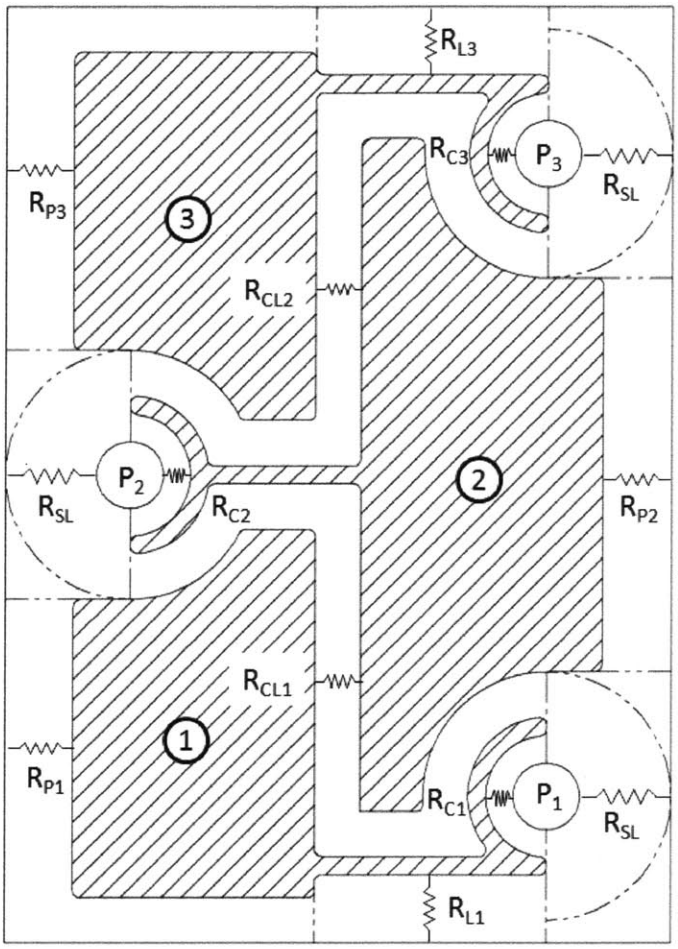

Figure 2-9: Resistance network regions

resistances is discussed in Appendix A.

For the resistance calculation, the geometry of the region is needed as well as the fluid viscosity and density. For these calculations, the viscosity and density of water at 20°C were used, 1.003×10^{-3} Ns/m^2 and 998 kg/m^3, respectively. For rectangular regions, (2.8) was used. The length and width of the rectangular lands were taken from the technical drawing in Appendix C. Calculations were only done for the shaft moving down toward the center of the flexible sheet, so the distance to the center of the land from the center of the flexible bearing material was used to calculate the arc length and combined with the nominal diameter of the bearing could be used to calculate the angle, θ, as shown in Figure 2-4. (2.15) was then used to calculate

the bearing gap for the land. For circular lands, a similar approach was used. The distance from the center of the circle was used to calculate the angle of the feature in the formed state. Then the angle was used to calculate the bearing gap at that location. The inner and outer radii from the drawing were used to calculate the resistance.

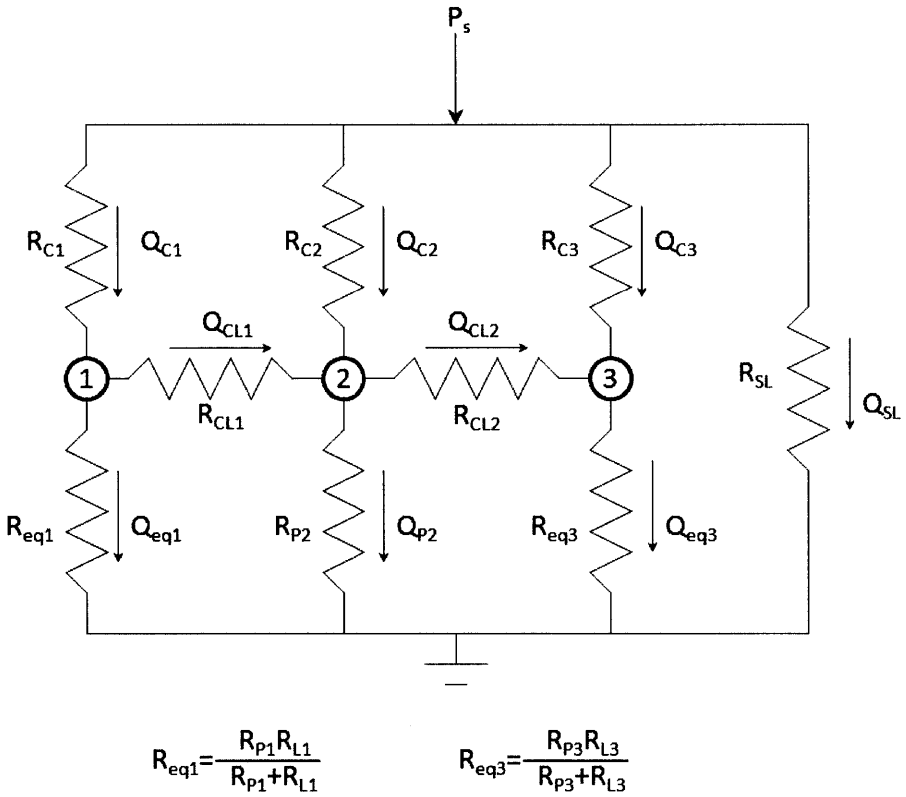

Figure 2-10: Resistance network model with the assumed flow direction

Using basic circuit theory, the pressures and flow rates can be solved for in a straight forward manner. Figure 2-10 shows the resistance network again but with assumed flow directions. The supply leakage flow is ignored for now because it can be solved for directly using the equation $P = QR$. R_{eq1} and R_{eq3} represent the equivalent resistance of the bearing pad lands and the leakage lands for bearing pads 1 and 3. Eight equations are needed to solve the network for the eight unknowns, Q_{C1}, Q_{C2}, Q_{C3}, Q_{CL1}, Q_{CL2}, Q_{eq1}, Q_{P2}, and Q_{eq3}. First Kirchhoff's Current Law can be applied to each node, which is equivalent to conservation of mass - the combined flows in and

out of each node must equal zero.

$$\begin{aligned} Q_{C1} - Q_{CL1} - Q_{eq1} &= 0 \\ Q_{C2} + Q_{CL1} - Q_{CL2} - Q_{P2} &= 0 \\ Q_{C3} + Q_{CL2} - Q_{eq3} &= 0 \end{aligned} \tag{2.32}$$

Next Kirchhoff's Voltage Law provides two more equations. These equations state that the net pressure change going around the upper loops is zero.

$$\begin{aligned} R_{C1}Q_{C1} + R_{CL1}Q_{CL1} - R_{C2}Q_{C2} &= 0 \\ R_{C2}Q_{C2} + R_{CL2}Q_{CL2} - R_{C3}Q_{C3} &= 0 \end{aligned} \tag{2.33}$$

Finally, three more equations are provided by realizing that the pressure drop across the compensator and the outlet must equal the supply pressure.

$$\begin{aligned} R_{C1}Q_{C1} + R_{eq1}Q_{eq1} &= P_s \\ R_{C2}Q_{C2} + R_{P2}Q_{P2} &= P_s \\ R_{C3}Q_{C3} + R_{eq3}Q_{eq3} &= P_s \end{aligned} \tag{2.34}$$

Equations (2.32), (2.33) and (2.34) form the following matrix equation which is easily solved by Matlab.

$$\begin{bmatrix} 1 & 0 & 0 & -1 & 0 & -1 & 0 & 0 \\ 0 & 1 & 0 & 1 & -1 & 0 & -1 & 0 \\ 0 & 0 & 1 & 0 & 1 & 0 & 0 & -1 \\ R_{C1} & -R_{C2} & 0 & R_{CL1} & 0 & 0 & 0 & 0 \\ 0 & R_{C2} & -R_{C3} & 0 & R_{CL2} & 0 & 0 & 0 \\ R_{C1} & 0 & 0 & 0 & 0 & R_{eq1} & 0 & 0 \\ 0 & R_{C2} & 0 & 0 & 0 & 0 & R_{P2} & 0 \\ 0 & 0 & R_{C3} & 0 & 0 & 0 & 0 & R_{eq3} \end{bmatrix} \begin{bmatrix} Q_{C1} \\ Q_{C2} \\ Q_{C3} \\ Q_{CL1} \\ Q_{CL2} \\ Q_{eq1} \\ Q_{P2} \\ Q_{eq3} \end{bmatrix} = \begin{bmatrix} 0 \\ 0 \\ 0 \\ 0 \\ 0 \\ P_s \\ P_s \\ P_s \end{bmatrix} \tag{2.35}$$

As mentioned earlier the supply leakage flow can be calculated using the circuit analogy mentioned in 2.1.1 such that $P = QR$. During design iterations it is worthwhile to examine the proportion of leakage flow to total flow. The proportion of leakage flow to total flow will vary based on the number of inlets, bearing arc, and load carrying efficiency. Large lands can be placed next to the inlets and grooves that route fluid to reduce leakage, but those lands will not improve the loads the bearing can support and will lower load carrying efficiency. Determining an appropriate amount of leakage flow is a trade off and requires engineering judgement.

The pressures of the nodes are found by multiplying the flow rates by the resistances. The three node pressures are calculated with the following equations.

$$\begin{aligned} P_1 &= R_{eq1} Q_{eq1} \\ P_2 &= R_{P2} Q_{P2} \\ P_3 &= R_{eq3} Q_{eq3} \end{aligned} \tag{2.36}$$

With these pressures, (2.17) is then be used to calculated the bearing pad forces. (2.19) along with the inlet pressure calculates the forces in the supply leakage region. The force at the inlet port is calculated by multiplying the inlet pressure by the inlet area. At this point the forces and flow rates have been solved for and dimensionless parameters are calculated to characterize the bearing.

Using this basic methodology, dimensions from CAD were input into a Matlab script and then the performance of the bearing was analyzed. Appendix B includes example code used to analyze this bearing.

Chapter 3

Results

3.1 Half Bearing Proof of Concept

For the halfbearing, features were machined into 2.54 mm thick adhesive-backed ultra high molecular weight (UHMW) polyethylene. In the proof of concept, the bearing was bonded into a 6061 T651 aluminum half cylinder. The half cylinder was turned in a lathe then cut in half. The design was sized to fit a precision ground 100 mm diameter shaft from another project. Initially, the bearing would not work and it was thought that the tube had collapsed when it was cut. The half cylinder was put in a hydraulic press to plastically deform the aluminum slightly which then allowed the shaft to float freely. Due to lack of measurement equipment, the amount of deformation was not quantified. The first half-bearing prototype is shown in Figure 3-1. In the picture the large diameter disc behind the shaft is an automotive brake rotor which was used as an axial rolling bearing to take up thrust loads. This initial prototype showed that the bearing design could support a shaft with a fluid film.

Samples of 6061 T651 aluminum tube with a nominal ID of 101.6 mm and OD of 127 mm were sent to NIST and measured on a Cordax CMM. Table 3.1 shows the diameter and cylindricity of the tube and the two halves after it was cut in half axially. As can be seen from the data, the tube opened up slightly after being cut. The change in diameter is significant compared to the designed bearing gap of 127 μm, which lends credence to the theory that though the inner diameter was machined

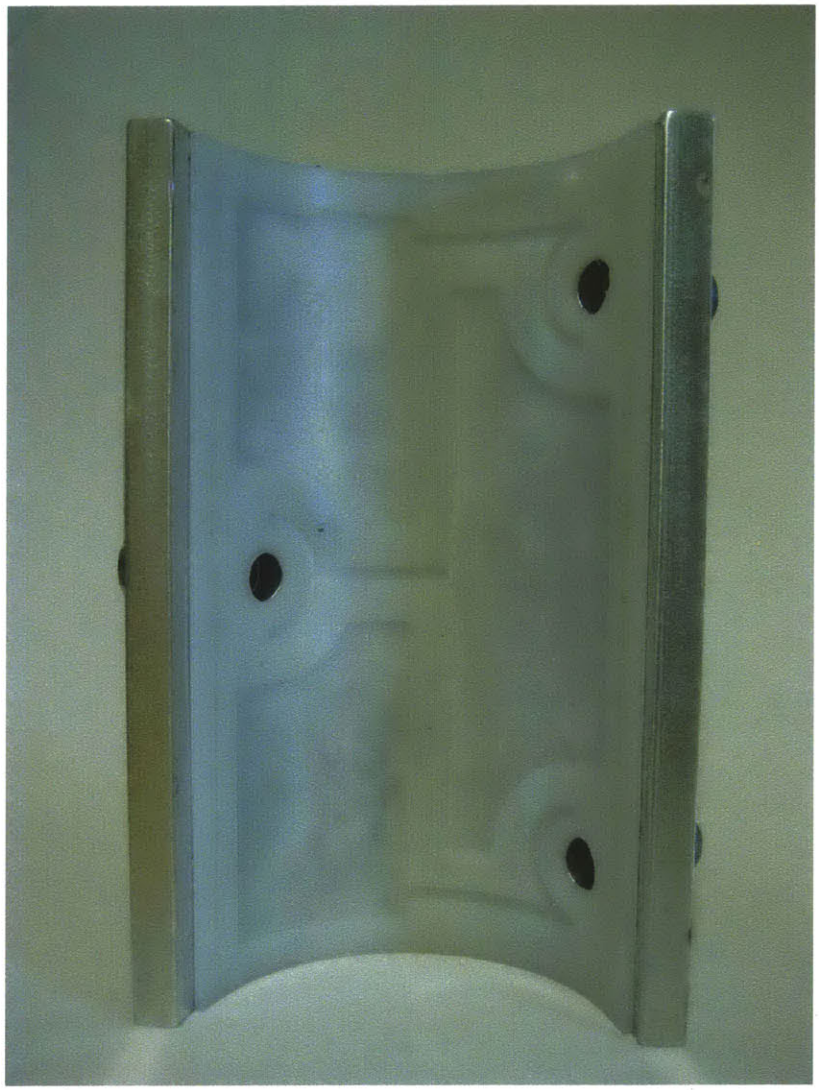

Figure 3-1: Proof of concept half bearing

properly, once the tube was cut in half, residual stresses caused the tube to distort and no longer hold the proper bearing gap.

3.2 Half Bearing Design

Upon finishing the proof of concept, a more compact design suitable for testing was designed so the performance of the bearing could be evaluated. A new aluminum housing was made by CNC machining a trough shape in a solid block of aluminum to prevent any warping issues due to residual stresses. A shorter shaft was machined to

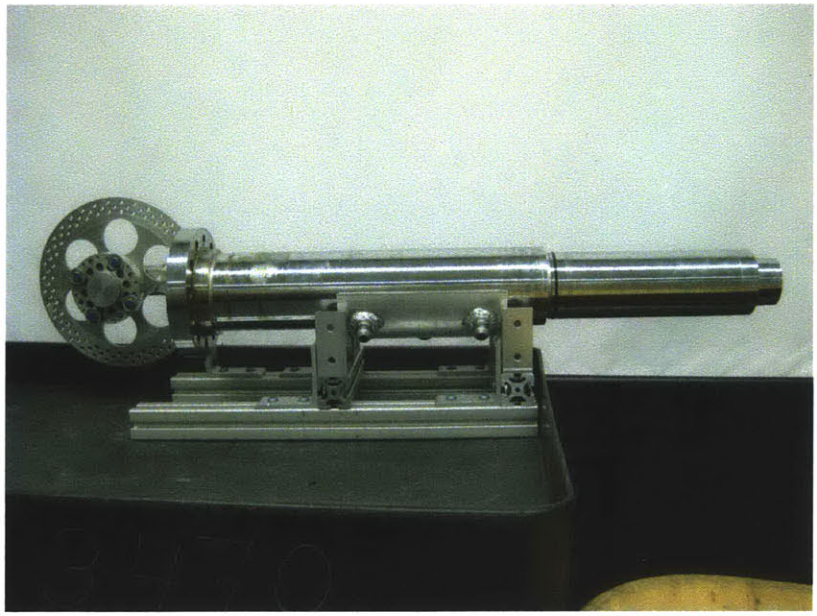

Figure 3-2: Setup for proof of concept half bearing (hoses removed for clarity)

Table 3.1: Measurements of 6061 T651 Tube and Half Tubes in mm

	Inner Surface		Outer Surface	
	⌀	Cyl	⌀	Cyl
Tube	101.521	0.211	126.818	0.242
Half 1	101.638	0.075	126.915	0.101
Half 2	101.653	0.054	127.015	0.079

provide a 127μm nominal gap. To address concerns about the UHMW delaminating from the aluminum, the aluminum housing, plastic and shaft were heated to 130°C in an oven with a 127μm sheet of shim stock between the shaft and the plastic to thermally form the plastic to the proper gap where the gap would ideally be the thickness of the shim stock. This process reduced the stresses in the plastic and helped the plastic to bond better to the aluminum. Figure 3-3 shows the plastic bonded into the aluminum housing after thermoforming. Figure 3-4 shows the new shaft. A new test setup was built for the bearing which includes a dedicated impeller pump, filter, flow meter, digital pressure readout, and ball valves for flow control in the fluid circuit. Air bearings are used to constrain the shaft axially. A compressed gas

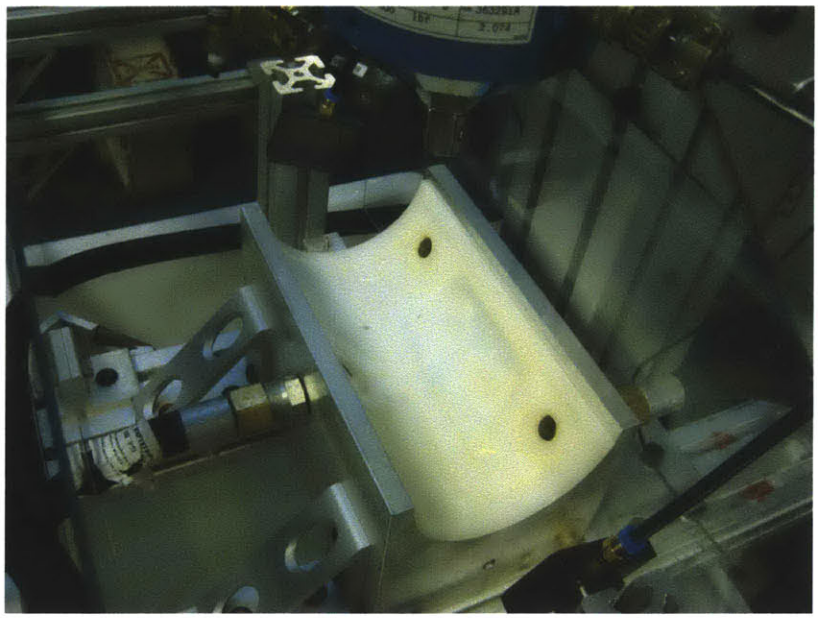

Figure 3-3: New housing with UHMW bearing adhered to it

cylinder was included to supply the air bearings to eliminate any noise that might have been introduced by a compressor. An Admet 5604 single column universal testing machine and an Interface 1210ACK-300-B load cell rated for 300 lbs are used for applying load to the shaft. The 5604 is driven by Admet's MTestQuattro software. Lion Precision U3B eddy current probes driven by ECL202 drivers measure the shaft location. All these components were installed on a stand alone cart fabricated from T-slot structural framing. The cart is on wheels to allow the test apparatus to be easily moved after the water reservoir has been filled. The MTestQuattro system records readings from the load cell, eddy current probes, and pressure gauge. Figure 3-5 shows the cart with the attached equipment.

Figure 3-6 shows the calculated and measured vertical load that the bearing supports. The calculated values come from the Matlab script in Appendix B solving the hydraulic resistance network model for the bearing. Figure 3-7 shows the stiffness of the bearing, or the slope of the previous curve, where the stiffness is defined as the change in force divided by the change in bearing gap, $k = \Delta F/\Delta h$. These two graphs demonstrate the hydraulic resistance model reasonably predicts the performance of the bearing and hence the design is deterministic. Figure 3-8 shows the measured

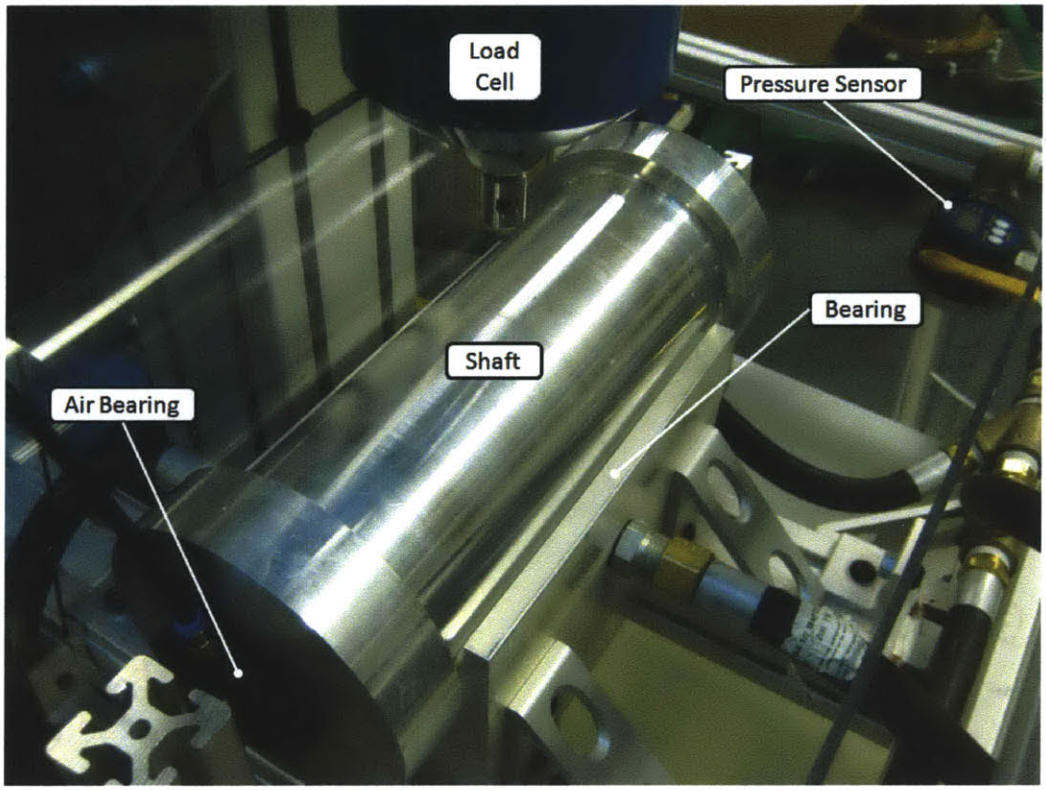

Figure 3-4: New smaller shaft with air bearings to maintain axial position

load carrying efficiency of the model, where the efficiency is calculated from (2.20). At 75% gap closure, the bearing has a 23% efficiency.

The bearing was also sent to NIST and measured on their Cordax CMM. The diameter of the bearing lands was measured as 99.719 mm with a cylindricity of 0.506 mm. The bearing was designed to have a nominal diameter of 99.746 mm. The cylindricity is almost four times the designed bearing gap. This raises questions about how the bearing can function so well with such poor precision! One theory is that compliance in the housing opens the bearing up slightly due to the fluid pressure such that the bearing can overcome form errors. Initial calculations estimate that the bearing may open up as much as 0.1mm due to the fluid pressure deforming the aluminum housing. The derivation and calculation of the housing deflection can be found in Appendix D

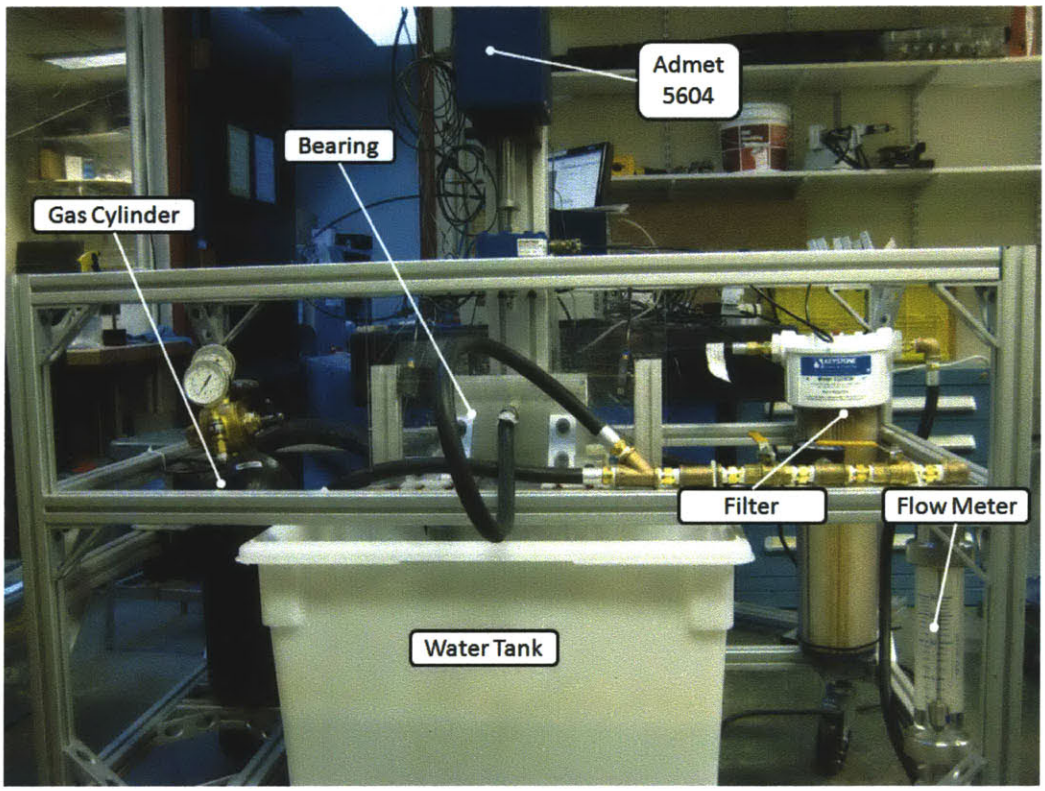

Figure 3-5: Final test setup

3.2.1 Sensitivity Study

Analysis was conducted to determine the effect of wrapping the groove further around the inlet holes. Figure 3-9 shows an example of increasing the amount the collector wraps around the inlet as well as the angle used to measure the additional length. The grooves were changed symmetrically, and the angle, ψ, is half the total amount of additional arc. Figure 3-10 shows the results of an analysis done for the same bearing with different additional angles of groove wrapping around the inlet. The curves shown are for the bearing operating at 15 psi inlet pressure. As the collector wraps further around the inlet, the load carrying efficiency increases. However, the additional load capacity comes at the cost of additional flow rate. Figure 3-11 shows how the specific flow rate, as defined in (2.23), increases with increasing angle of additional wrap.

Another analysis was done to examine the effect of the collector land thickness,

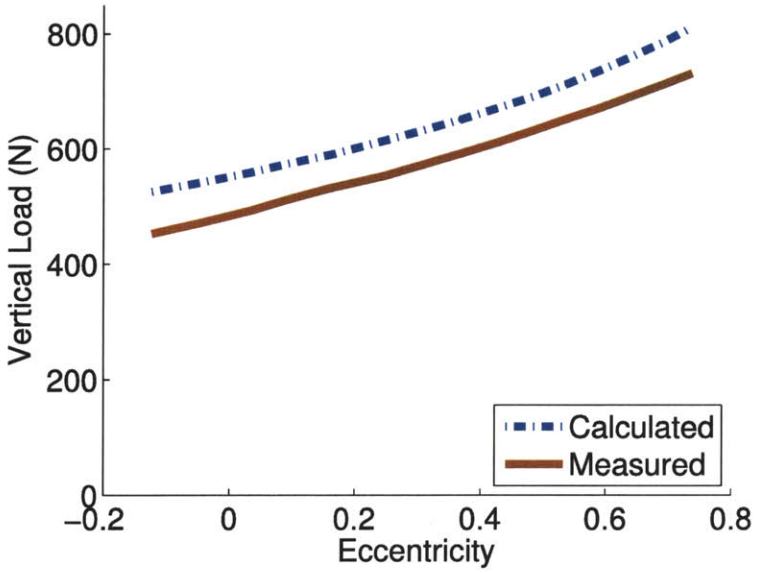

Figure 3-6: Comparison of calculated and measured load

T, shown in Figure 3-9. This land can be adjusted to change the fluid resistance of the compensator and thus the resistance ratio, which is defined as the ratio of the resistance of the inlet to the resistance of the outlet. Figure 3-12 shows the results. The abscissa is the resistance ratio at zero eccentricity averaged over the three pockets. The initial specific stiffness is calculated as a change in load carrying efficiency for a change in eccentricity from 0 to 0.01 divided by the change in eccentricity. The reported load carrying efficiency is calculated at 75% gap closure. As can be seen, varying the resistance ratio trades load carrying efficiency for stiffness, and both cannot be optimized simultaneously by means of the resistance ratio alone. Figure 3-13 shows the product of the two curves in Figure 3-12 plotted against the resistance ratio. The maximum occurs at a resistance ratio of 0.4651.

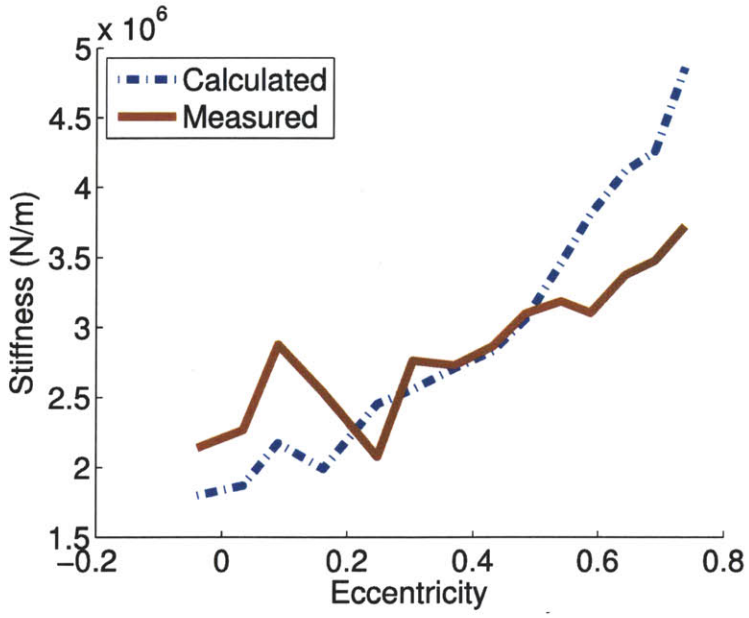

Figure 3-7: Comparison of calculated and measured stiffness

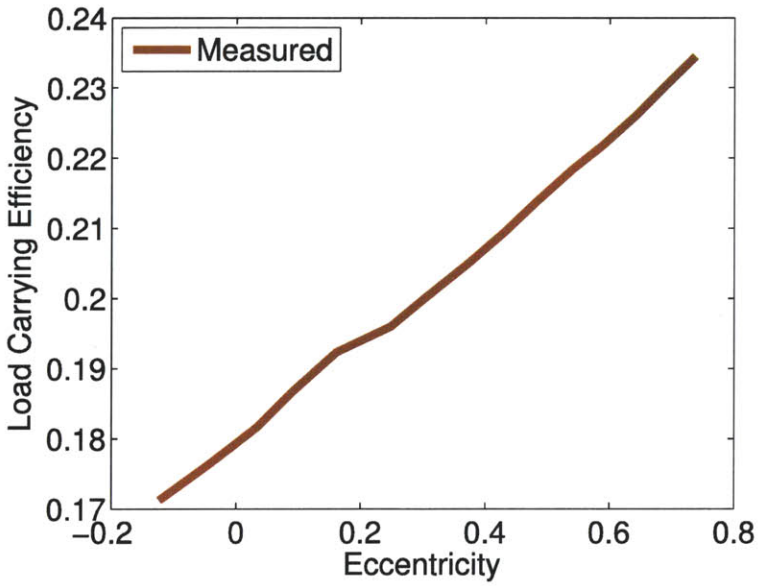

Figure 3-8: Load carrying efficiency

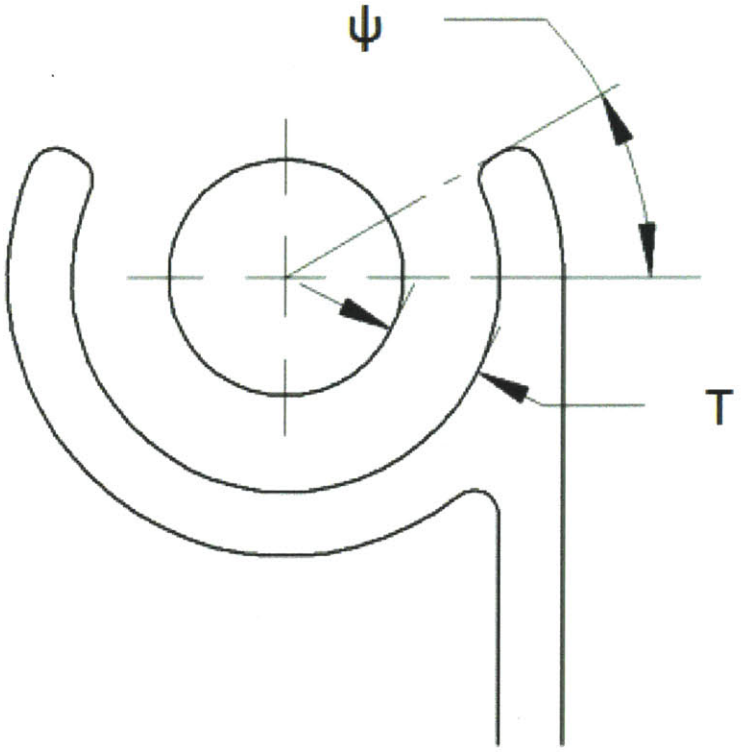

Figure 3-9: Diagram of collector

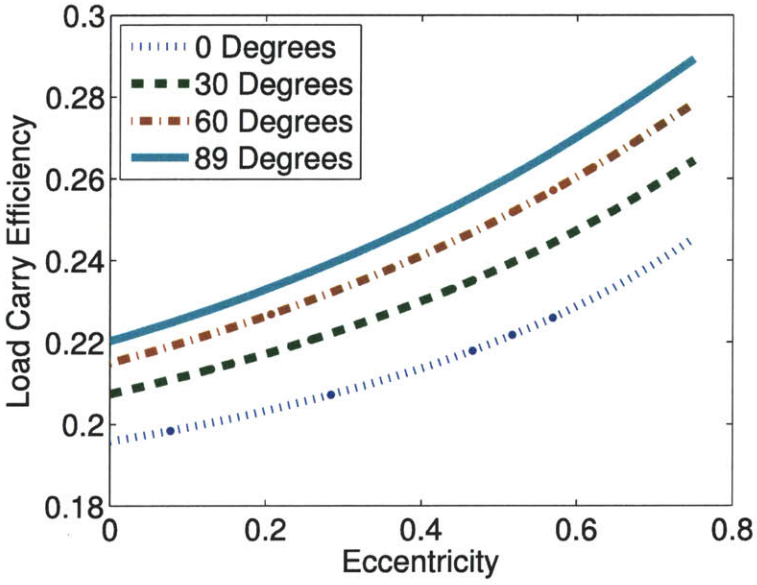

Figure 3-10: Load sensitivity to additional collector land angle, *psi*

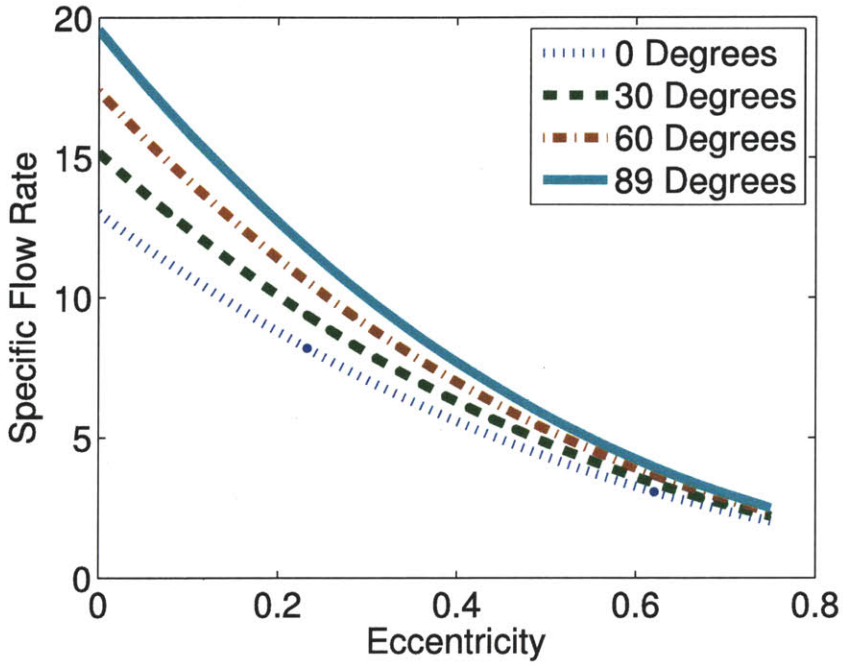

Figure 3-11: Flow sensitivity to additional collector land angle, ψ

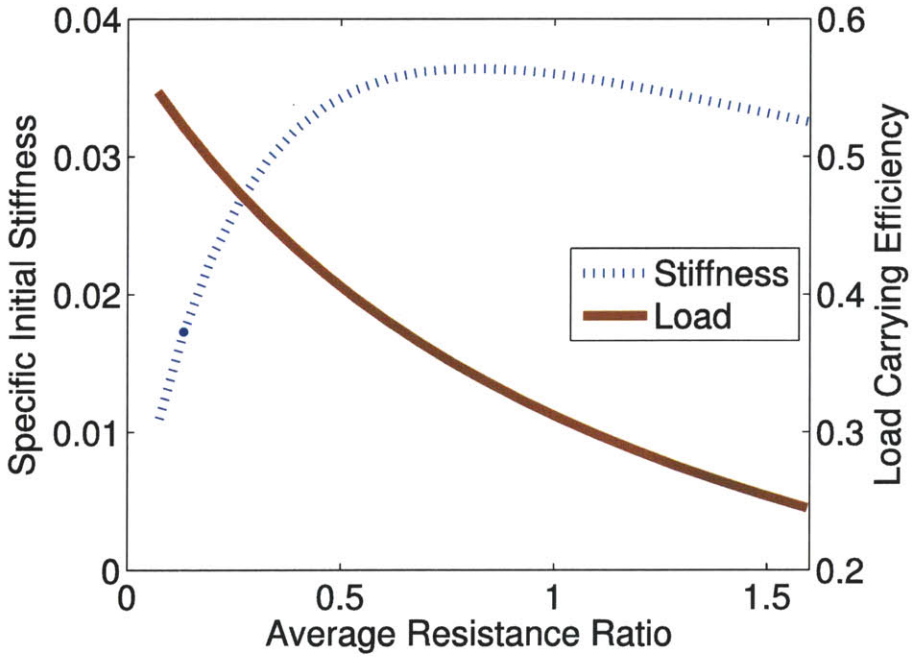

Figure 3-12: Bearing performance sensitivity to resistance ratio

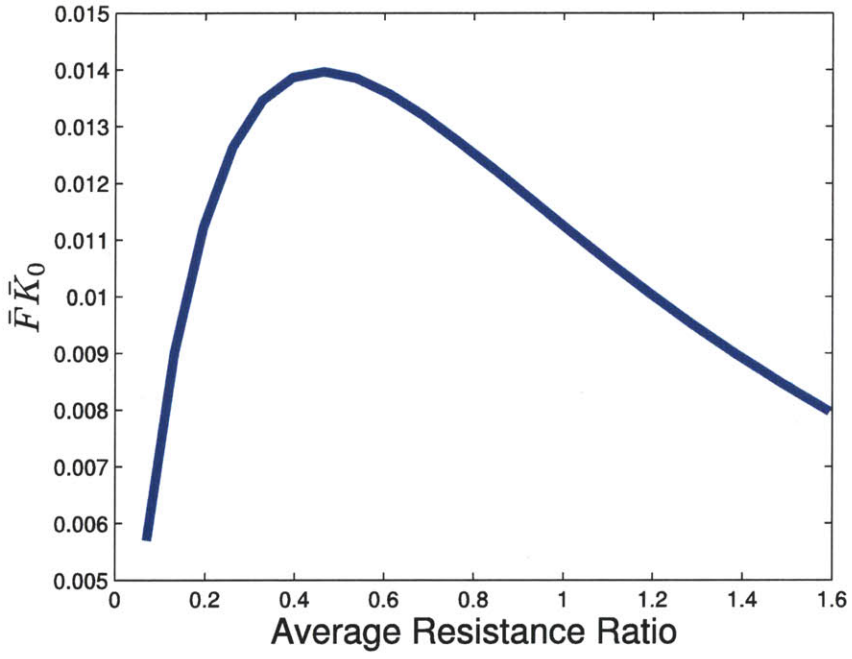

Figure 3-13: Initial specific stiffness times load carrying efficiency plotted against resistance ratio

Chapter 4

Conclusions

This work demonstrates the deterministic design theory for a surface self compensated hydrostatic bearing covering less than 180° of the shaft surface. This paper evaluates just one half of a bearing to support a horizontal heavy shaft and analyzes the sensitivities of the bearing performance to the some of the design parameters. In practice though the bearings could be paired to provide preload on the other side of the shaft. Also a method to manufacture such a bearing is presented. This bearing design, being a partial arc, facilitates installation and repair of hydrostatic bearings in support of large shafts since it does not need to be slid over the end of the shaft.

4.1 Future Work

Future work will investigate the hydrodynamic performance of this type of bearing. The ultimate goal is to be able to produce a low cost bearing which runs hydrostaticly at low shaft speeds and hydrodynamically at high shaft speeds to reduce operating cost by allowing pumping power to be reduced.

Other manufacturing methods should also be pursued to reduce the cost and time to make these bearings. Specifically, examining methods that would allow an as-extruded tube, casting, or forging to be used as the bearing housing would be significantly cheaper than using a CNC machined trough. Table 3.1 shows that the cylindricity of the as-extruded aluminum half tube is two orders of magnitude lower

than the UHMW thickness. UHMW may be able to be thermoformed to fill in the errors in the tube while also replicating a master shaft diameter.

Other topologies should also be investigated. The pattern of grooves presented in this thesis is by no means the only pattern. Other topologies potentially have better performance or could be optimized for different applications.

Finally, the bearing has been shown to be very robust. Further investigation is needed to understand how the bearing can still function with so much form error.

Appendix A

Discretization of the Surface Topology

A.1 Fluid Resistances

The surface of the bearing needs to be divided up into regions and a resistance value needs to be determined for the regions. The size of the regions requires some balancing. On the one hand, if the regions are too large, the results may become unreliable especially if a single gap measurement is used for a large area. On the other hand, as the regions get smaller, computational time is increased. One could imagine that if very fine regions are used, the problem turns into CFD. The power in the lumped resistance network lies in the ease of setting up the problem and speed of computation without sacrificing accuracy significantly. As part of the effort to balance fidelity with ease, some regions are double counted and some are not counted at all to make setting up the problem easier. The following subsections will show how the surface was divided up into regions and turned into fluid resistances.

Concerning nomenclature, the subscript 'C' indicates that the resistance is for the compensator, 'CL' for cross leakage between nodes, 'P' for leakage out of the load bearing pad, 'L' for leakage, and 'SL' for supply leakage directly from the inlet to the bearing outlet. The first numerical subscript indicates which node the region is related to. The second numerical subscript after the underscore indicates a subregion

within that category of regions. The resistor icons indicates the assumed direction of flow. Tilting of the shaft was ignored, so all gap measurements come from (2.15).

A.1.1 Compensator

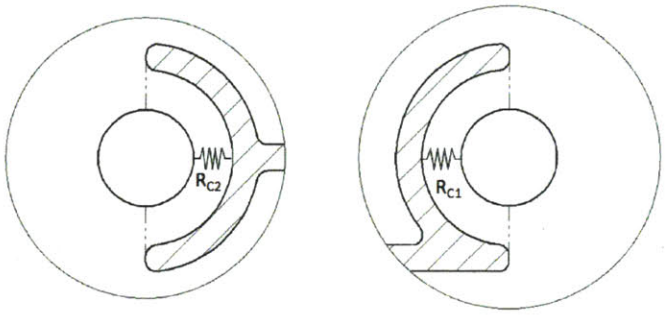

Figure A-1: Compensator resistance regions

Figure A-1 shows the regions used for the compensator resistance for inlet 1 on the right and inlet 2 on the left. Inlet 3 is the mirror image of inlet 1. This region is treated as a flow going radially outward from half an annululus per (2.13). The gap at the center of the inlet was used as the gap for this region.

A.1.2 Cross Leakage

Figure A-2 shows the regions used for the leakage between the recessed regions shown with the hatching. The cross-hatched regions indicate areas that were ignored. The fluid flow is parallel to the resistor icons. The bolded lines indicate the edges of the regions being discussed. The dot-filled regions indicate areas that were double counted. R_{CL1_1}, R_{CL1_2}, R_{CL1_3}, R_{CL2_1}, R_{CL2_2}, and R_{CL2_3} are all treated as rectangular parallel plates according to (2.8). The gap at the center of the region was used in calculating the resistances. R_{CL1_4} and R_{CL2_4} are treated as a quarter of an annular region flowing radially outward. These regions slightly overlap with R_{CL1_3} and R_{CL2_3} as shown by the dotted areas. The gap at the center of P_{1_1} and P_{3_1} shown in Figure A-4 were used for calculating the resistances of these regions. R_{CL1_5}

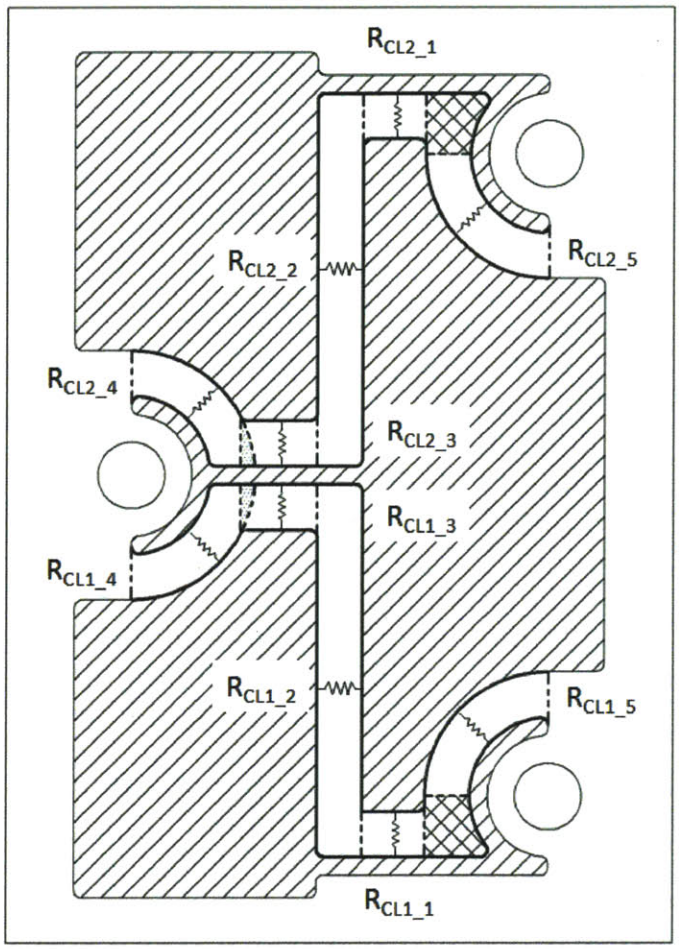

Figure A-2: Cross leakage resistance regions (Cross hatched regions are ignored)

and R_{CL2_5} are also treated as a quarter of an annular region flowing radially outward. The gap at the center of P_{2_1} shown in Figure A-4 was used for the calculating the resistances of these regions.

A.1.3 Bearing Pad

Figure A-3 shows the regions used for the flow from the bearing pads. The bearing pad regions were treated as rectangular parallel plates as in (2.8). The bearing pad regions for node 1 and 3, R_{P1_1}, R_{P1_2}, R_{P2_1}, and R_{P2_2}, used the bearing gap at P_{1_1} and P_{3_1} to calculate the resistances. The bearing pad regions for node 2, R_{P2}, used the bearing gap at P_{2_1}.

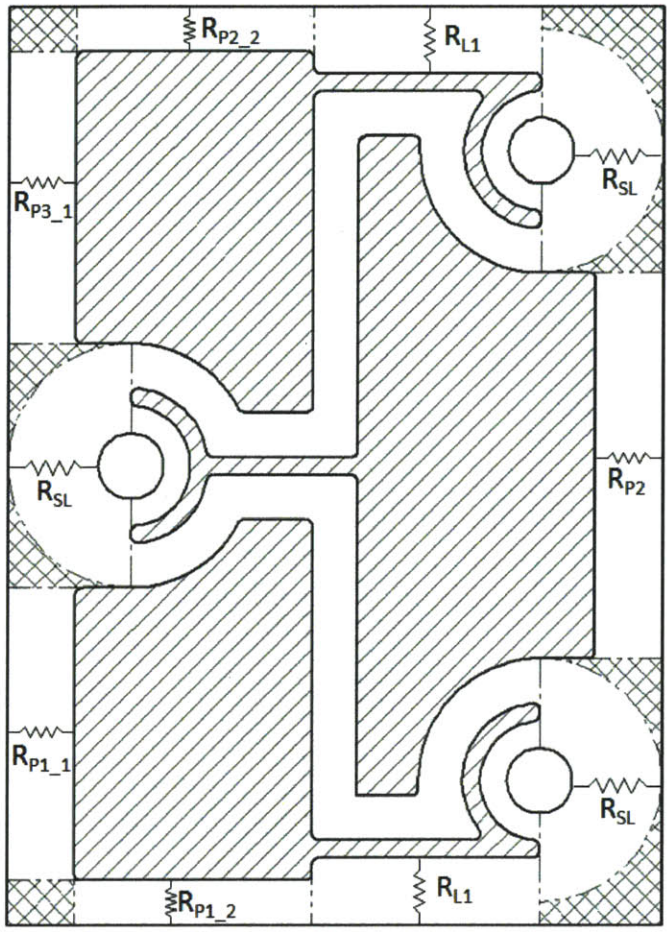

Figure A-3: Bearing pad, leakage and supply leakage resistance regions

A.1.4 Leakage

Leakage regions were defined as in Figure A-3. These regions account for leakage from the grooves connecting the collectors to their respective bearing pads and were separated from the bearing pad regions to be able to track flows that did not contribute to bearing performance. For these leakage regions the gap at the center of the inlet was used for computing the resistance.

A.1.5 Supply Leakage

The leakage directly from the inlets to atmospheric pressure were tracked to be able to calculate total flow rate needed from the pump. The regions were treated as half

annular regions per (2.13). The gap at the center of the inlet was used for these resistances.

A.2 Load Areas

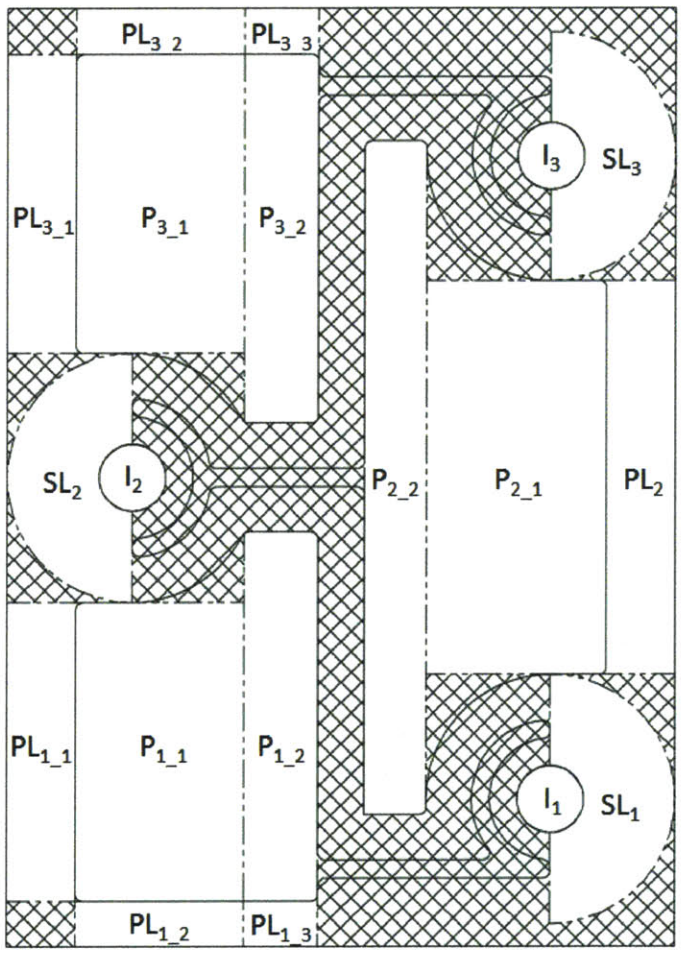

Figure A-4: Load carrying regions

For calculating the force from the bearing, the load carrying areas were broken up into regions and the load was calculated similar to (2.17). The recessed bearing pad regions are denoted by 'P' with the subscript numerals similar to the resistance nomenclature. The bearing pad lands, or lands next to the bearing pads, are marked 'PL'. The inlet ports are marked 'I'. The assumed region for supply leakage are labeled

'SL'. Angles were assumed and used to calculate the force component in the vertical direction for each region.

A.2.1 Bearing Pads

The recessed bearing pads were each divided into two regions shows in Figure A-4. The cross-hatched areas in Figure A-4 were not considered in the calculation of forces. The force was considered to be applied from the center of the regions for calculating the angle the force acted in. The forces in the bearing pads were calculated by multiplying the recess pressure by the area.

A.2.2 Bearing Pad Lands

The bearing pad lands for node 1 and 3 were divided into three parts as can be seen in Figure A-4. The pressure in these pad lands were considered to be decreasing linearly from the bearing pad recess pressure, so the pad land forces were calculated as half the recess pressure multiplied by the area similar to (2.17). The forces from PL_{1_1}, PL_{1_2}, PL_{3_1}, and PL_{3_2} were treated as acting at the same angle as P_{1_1} and P_{3_1}. PL_{1_3} and PL_{3_3} were treated as acting at the same angle as P_{1_2}. PL_2 was considered to be acting at the same angle as P_{2_1}.

A.2.3 Inlet ports

The supply pressure was multipled by the circular area to calculate the force applied by the inlet ports. The forces were considered to be applied at the center of the inlet port for the purposes of determining the angle of the force. Given the symmetry of the bearing, the loads from the inlet ports are considered to be the same for all inlets.

A.2.4 Supply Leakage

The supply leakage regions were modeled as a half an annuli. Though the region is rectangular in shape, the flow goes in multiple directions. The forces were calculated

using (2.19). For determining the angle of the force, the force was approximated as coming from the center of the inlet. Like the inlet port forces, the forces for the supply leakage regions were considered to be the same for all the inlets.

Appendix B

Matlab Code

```
function [Fv, Feff, e, Qtotal] = halfbearing(P, h)
%------INPUTS------
%For lengths of hydraulic regions, 'L' is in the direction of the ...
    assumed fluid flow direction. 'w' is the dimension ...
    perpendicular to the flow.
Ps = P* 6894.75728;      %[Pa], Supply pressure
D = 0.099719;            %[m], NIST measured Surface Diameter
L = 2*.1028956;          %[m], Bearing Length
ho = (D-3.917*.0254)/2; %[m], Measured clearance
s_i = .04598;            %[m], Distance between the centerline and ...
    inlet
ri = .00735;             %[m], Compensator inner radius
ro = .01335;             %[m], Compensator outer radius
Lcl_1 = .01;             %[m], Cross leakage length of region 1
wcl_1 = .01384;          %[m], Cross leakage width of region 1
Lcl_2 = .010;            %[m], Cross leakage length of region 2
wcl_2 = .0819;           %[m], Cross leakage width of region 2
Lcl_3 = .010;            %[m], Cross leakage length of region 3
wcl_3 = .01641;          %[m], Cross leakage width of region 3
ricl_4 = .01735;         %[m], Cross leakage inner radius of ...
    region 4
```

```
18 rocl_4 = .02735;          %[m], Cross leakage outer radius of ...
       region 4
19 ricl_5 = .01735;          %[m], Cross leakage inner radius of ...
       region 5
20 rocl_5 = .02735;          %[m], Cross leakage outer radius of ...
       region 5
21 Lpl1_1 = .015;            %[m], Pocket land region 1 length
22 Lpl1_2 = .01;             %[m], Pocket land region 2 length
23 Lp1_1 = .05333 - wcl_3;   %[m], Pocket1 region 1 length
24 wp1_1 = .06555;           %[m], Pocket1 region 1 width
25 Lp1_2 = wcl_3;            %[m], Pocket1 region 2 length
26 wp1_2 = .0809;            %[m], Pocket1 region 2 width
27 Lp2_1 = .05333 - wcl_1;   %[m], Pocket2 region 1 length
28 wp2_1 = .08639;           %[m], Pocket2 region 1 width
29 Lp2_2 = wcl_1;            %[m], Pocket2 region 2 length
30 wp2_2 = .14779;           %[m], Pocket2 region 2 width
31 Ll1_1 = .015;             %[m], Pocket1 leakage length for region 1
32 wl1_1 = .05098;           %[m], Pocket1 leakage width for region 1
33 rol1_2 = .02735;          %[m], Pocket1 leakage outer radius for ...
       region 2
34 ril1_2 = .01735;          %[m], Pocket1 leakage inner radius for ...
       region 2
35 rol2 = .02735;            %[m], Pocket2 leakage outer radius
36 ril2 = .01735;            %[m], Pocket2 leakage inner radius
37 rosl = .02735;            %[m], Supply leakage outer radius
38 risl = .00735;            %[m], Supply leakage inner radius
39
40 %------CONSTANTS------
41 global mu1 rho
42 mu1 = 1.003e-3;           %[Ns/m^2], Viscosity
43 rho = 998;                %[kg/m^3], Density
44
45 %------CALCULATIONS------
46 gammac = s_i/(pi*D)*360;                                    ...
       %[degrees], Angle of compensator
```

```
47 gammap1_1 = (Lcl1_2/2 + Lp1_2 + Lp1_1/2)/(pi*D)*360;     ...
       %[degrees], Angle of pocket1 region 1
48 gammap1_2 = (Lcl_2/2 + Lp1_2/2)/(pi*D)*360;              ...
       %[degrees], Angle of pocket1 region 2
49 gammap2_1 = (Lcl_2/2 + Lp2_2 + Lp2_1/2)/(pi*D)*360;      ...
       %[degrees], Angle of pocket2 region 1
50 gammap2_2 = (Lcl_2/2 + Lp2_2/2)/(pi*D)*360;              ...
       %[degrees], Angle of pocket2 region 2
51 e = (ho - h)/ho;                                         %[], ...
       Eccentricity
52 hc = ho * (1-e*cos(gammac*(pi/180)));                    %[m], ...
       Bearing gap at collector
53 hp1_1 = ho * (1-e*cos(gammap1_1*(pi/180)));              %[m], ...
       Bearing gap at pocket1 region 1
54 hp1_2 = ho * (1-e*cos(gammap1_2*(pi/180)));              %[m], ...
       Bearing gap at pocket1 region 2
55 hp2_1 = ho * (1-e*cos(gammap2_1*(pi/180)));              %[m], ...
       Bearing gap at pocket2 region 1
56 hp2_2 = ho * (1-e*cos(gammap2_2*(pi/180)));              %[m], ...
       Bearing gap at pocket2 region 2
57
58 %Calculate hydraulic resistances
59 %Compensators
60 Rc1 = Rcirc(ro, ri, hc)*2;
61 Rc2 = Rc1;
62 Rc3 = Rc1;
63 %Cross Leakage
64 Rcl_1 = Rrect(Lcl_1, wcl_1, hp2_2);
65 Rcl_2 = Rrect(Lcl_2, wcl_2, h);
66 Rcl_3 = Rrect(Lcl_3, wcl_3, hp1_2);
67 Rcl_4 = Rcirc(rocl_4, ricl_4, hp1_1) * 4;
68 Rcl_5 = Rcirc(rocl_5, ricl_5, hp2_1) * 4;
69 Rcl1 = 1/((1/Rcl_1)+(1/Rcl_2)+(1/Rcl_3)+(1/Rcl_4)+(1/Rcl_5));
70 Rcl2 = Rcl1;
71 %Bearing Pads
72 Rp1_1 = Rrect(Lpl1_1, wp1_1, hp1_1);
```

```
Rp1_2 = Rrect(Lpl1_2, Lp1_1+Lp1_2, hp1_1);
Rp1 = 1/((1/Rp1_1)+(1/Rp1_2));
Rp2 = Rrect(Lpl1_1, wp2_1, hp2_1);
Rp3 = Rp1;
%Leakage
Rl1 = Rrect(Ll1_1, wl1_1, hc);
Rl3 = Rl1;
%Equivalent Resistances
Req1 = 1/((1/Rp1)+(1/Rl1));
Req2 = Rp2;
Req3 = 1/((1/Rp3)+(1/Rl3));
%Supply Leakage
Rsl1 = Rcirc(rosl, risl, hc)*2;
Rsl2 = Rcirc(rosl, risl, hc)*2;
Rsl = 1/((2/Rsl1)+1/(Rsl2));


%Matrix equations to simultaneously solve for the flow rates
K = [1    0    0    -1   0    -1   0    0;
     0    1    0    1    -1   0    -1   0;
     0    0    1    0    1    0    0    -1;
     Rc1  -Rc2 0    Rcl1 0    0    0    0;
     0    Rc2  -Rc3 0    Rcl2 0    0    0;
     Rc1  0    0    0    0    Req1 0    0;
     0    Rc2  0    0    0    0    Req2 0;
     0    0    Rc3  0    0    0    0    Req3;];

f = [0; 0; 0; 0; 0; Ps; Ps; Ps];
Q = K\f;            %[m^3/s], [Qc1; Qc2; Qc3; Qcl1; Qcl2; Qeq1; ...
    Qeq2; Qeq3]
Peq1 = Q(6) * Req1; %[Pa], Pressure in bearing pad 1/leakage ...
    equivalent region
Peq2 = Q(7) * Req2; %[Pa], Pressure in bearing pad 2/leakage ...
    equivalent region
Peq3 = Q(8) * Req3; %[Pa], Pressure in bearing pad 3/leakage ...
    equivalent region
```

```
105 Qp1 = Peq1 / Rp1;    %[m^3/s], Flow in bearing pad 1
106 Qp2 = Peq2 / Rp2;    %[m^3/s], Flow in bearing pad 2
107 Qp3 = Peq3 / Rp3;    %[m^3/s], Flow in bearing pad 3
108 Ql1 = Peq1 / Rl1;    %[m^3/s], Leakage flow in bearing pad 1
109 Ql3 = Peq3 / Rl3;    %[m^3/s], Leakage flow in bearing pad 3
110 Qsl = Ps / Rsl;      %[m^3/s], Supply leakage flow
111 Qleak = Ql1 + Ql3 + Qsl;                %[m^3/s], Total Leakage flow
112 Qtotal = Q(1) + Q(2) + Q(3) + Qsl;      %[m^3/s], Total flow
113
114 %Calculate Bearing Forces
115 %Inlet1
116 Fi1 = Ps * pi * ri^2;                  %[N], Force in inlet
117 Fs1 = (pi*Ps*(rosl^2-risl^2)/(2*log(rosl/risl))-pi*Ps*risl^2)/2; ...
        %[N], Force in supply leakage region
118 Fi = Fi1 + Fs1;                       %[N], Total force for inlet area
119 Fiv = Fi * cos(gammac*pi/180);        %[N], Total vertical force ...
    from one inlet
120 %Pocket1
121 Fp1_1 = Peq1 * Lp1_1 *wp1_1;     %[N], Force in the pocket region 1
122 Fp1_2 = Peq1 * Lp1_2 *wp1_2;     %[N], Force in the pocket region 2
123 Fp1_3 = Peq1 * Lpl1_1 * wp1_1 / 2;     %[N], Force in the pocket ...
    land region1
124 Fp1_4 = Peq1 * Lpl1_2 * Lp1_1 / 2;     %[N], Force in the pocket ...
    land region2
125 Fp1_5 = Peq1 * Lpl1_2 * Lp1_2 / 2;     %[N], Force in the pocket ...
    land region3
126 Fp1 = Fp1_1 + Fp1_2 + Fp1_3 + Fp1_4 + Fp1_5;     %[N], Total force ...
    in pocket1
127 Fp1v = Fp1_1 * cos(gammap1_1*pi/180) + Fp1_2 * ...
    cos(gammap1_2*pi/180) + Fp1_3 * cos(gammap1_1*pi/180) + Fp1_4 ...
    * cos(gammap1_1*pi/180) + Fp1_5 * cos(gammap1_2*pi/180);     ...
    %[N], Vertical force from pocket1
128 %Pocket2
129 Fp2_1 = Peq2 * Lp2_1 *wp2_1;     %[N], Force in the pocket region 1
130 Fp2_2 = Peq2 * Lp2_2 *wp2_2;     %[N], Force in the pocket region 2
```

```
131 Fp2_3 = Peq2 * Lpl1_1 * wp2_1 / 2;     %[N], Force in the pocket ...
       land region
132 Fp2 = Fp2_1 + Fp2_2 + Fp2_3;     %[N], Total force in pocket2
133 Fp2v = Fp2_1 * cos(gammap2_1*pi/180) + Fp2_2 * ...
       cos(gammap2_2*pi/180) + Fp2_3 * cos(gammap2_1*pi/180);     ...
       %[N], Vertical force from pocket2
134 %Pocket3
135 Fp3_1 = Peq3 * Lp1_1 *wp1_1;     %[N], Force in the pocket region 1
136 Fp3_2 = Peq3 * Lp1_2 *wp1_2;     %[N], Force in the pocket region 2
137 Fp3_3 = Peq3 * Lpl1_1 * wp1_1 / 2;     %[N], Force in the pocket ...
       land region1
138 Fp3_4 = Peq3 * Lpl1_2 * Lp1_1 / 2;     %[N], Force in the pocket ...
       land region2
139 Fp3_5 = Peq3 * Lpl1_2 * Lp1_2 / 2;     %[N], Force in the pocket ...
       land region3
140 Fp3 = Fp3_1 + Fp3_2 + Fp3_3 + Fp3_4 + Fp3_5;     %[N], Total force ...
       in pocket1
141 Fp3v = Fp3_1 * cos(gammap1_1*pi/180) + Fp3_2 * ...
       cos(gammap1_2*pi/180) + Fp3_3 * cos(gammap1_1*pi/180) + Fp3_4 ...
       * cos(gammap1_1*pi/180) + Fp3_5 * cos(gammap1_2*pi/180);     ...
       %[N], Vertical force from pocket1
142
143 Fv = Fp1v + Fp2v + Fp3v + 3*Fiv;     %[N], Total vertial force
144 F = Fp1 + Fp2 + Fp3 + 3*Fi;          %[N], Total force
145
146 %Calculate Resistance Ratios
147 zeta1 = Rc1 / Rp1;
148 zeta2 = Rc2 / Rp2;
149 zeta3 = Rc2 / Rp3;
150
151 %Ratio of Leakage Resistance : Compensator Resistance
152 ksi1 = Rl1 / Rc1;
153 ksi2 = Rl2 / Rc2;
154 ksi3 = Rl3 / Rc3;
155
156 %Bearing Parameters
```

```
157 Feff = Fv / (Ps * D * L);    %Load Carrying Efficiency
158 Qspec = Qtotal / (Ps * pi * D * ho^3 / (12 * mu1 * L));    ...
        %Specific Flow Rate
159
160 %------OUTPUT------
161 fprintf('Qc1 = %4.3e m^3/s \nQc2 = %4.3e m^3/s \nQc3 = %4.3e ...
        m^3/s \nQcl1 = %4.3e m^3/s \nQcl2 = %4.3e m^3/s \nQp1 = %4.3e ...
        m^3/s \nQp2 = %4.3e m^3/s \nQp3 = %4.3e m^3/s \nQl = %4.3e ...
        m^3/s \n', Q(1:5),Qp1, Qp2, Qp3, Ql)
162 fprintf('Pocket1 Resistance Ratio = %4f\nPocket2 Resistance Ratio ...
        = %4f\nPocket3 Resistance Ratio = %4f\n', zeta1, zeta2, zeta3)
163 fprintf('Pocket1 Leakage Ratio = %4f\nPocket3 Leakage Ratio = ...
        %4f\n', ksi1, ksi3)
164 fprintf('Load Carrying Efficiency = %4f\nSpecific Flow Rate = ...
        %4f\n', Feff, Qspec)
165 fprintf('Total Vertical Force = %4f N\nTotal flow rate = %4f ...
        m^3/s\nAt eccentricity %4f\n\n', Fv, Qtotal, e)
166 end
167
168 %------External Functions------
169 % These are copies of functions called to calculate the ...
        resistance of various regions
170
171 % function R = Rrect(L, w, h)
172 % %Compute the hydraulic resistance of a rectangular region
173 % global mu1
174 % R = 12*mu1*L/(h^3 * w);
175 % end
176
177 % function R = Rcirc(ro, ri, h)
178 % %Compute the hydraulic resistance of an annular region
179 % global mu1
180 % R = 6*mu1*log(ro/ri)/(pi*h^3);
181 % end
```

Appendix C

Technical Drawing

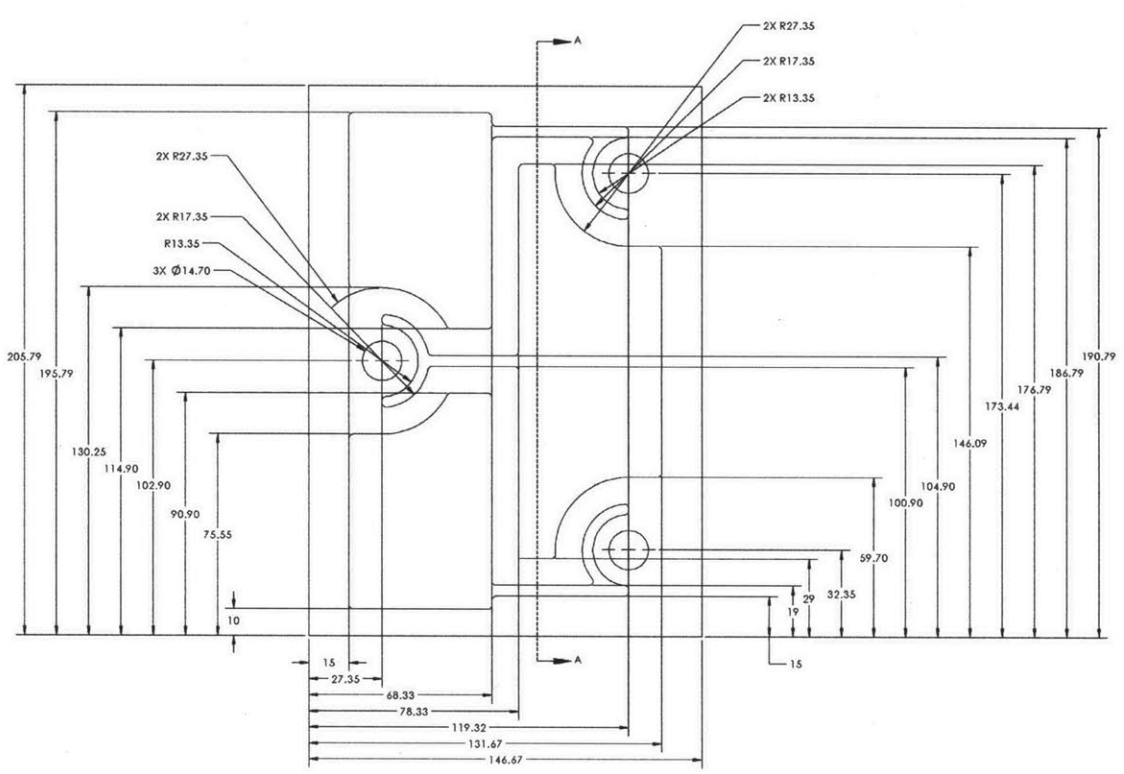

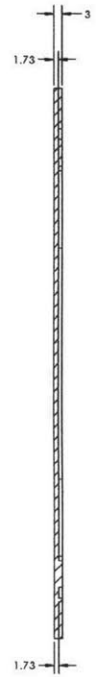

SECTION A-A

UNLESS OTHERWISE SPECIFIED:
DIMENSIONS ARE IN MM
TOLERANCES
FRACTIONAL ±
ANGULAR: MACH ± BEND ±
TWO PLACE DECIMAL ±
THREE PLACE DECIMAL ±
MATERIAL: UHMW HDPE
FINISH
DO NOT SCALE DRAWING

NAME DATE
DRAWN
CHECKED
ENG APPR.
MFG APPR.
Q.A.
COMMENTS

NEXT ASSY USED ON
APPLICATION

PROPRIETARY AND CONFIDENTIAL
THE INFORMATION CONTAINED IN THIS DRAWING IS THE SOLE PROPERTY OF MR. ANY REPRODUCTION IN PART OR AS A WHOLE WITHOUT THE WRITTEN PERMISSION OF MR IS PROHIBITED.

TITLE:
BEARING LINER

SIZE C | DWG. NO. 301-0000 | REV 00

SCALE:1:1 WEIGHT: SHEET 1 OF 2

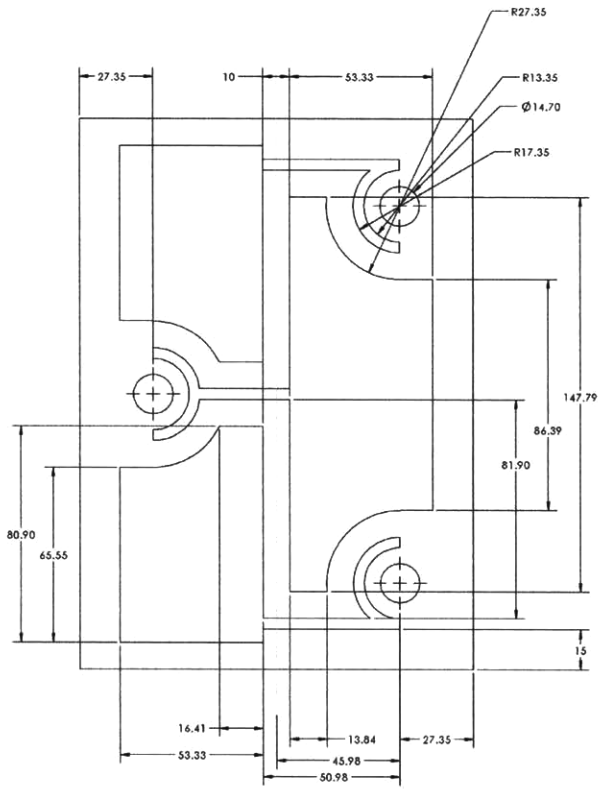

RESISTANCE NETWORK DIMENSIONS
(ALL DIMENSIONS REFERENCE)

TITLE:
BEARING LINER

SIZE DWG. NO. REV
C 301-0000 00

SCALE: 1:1 WEIGHT: SHEET 2 OF 2

Appendix D

Calculation of Housing Deflection

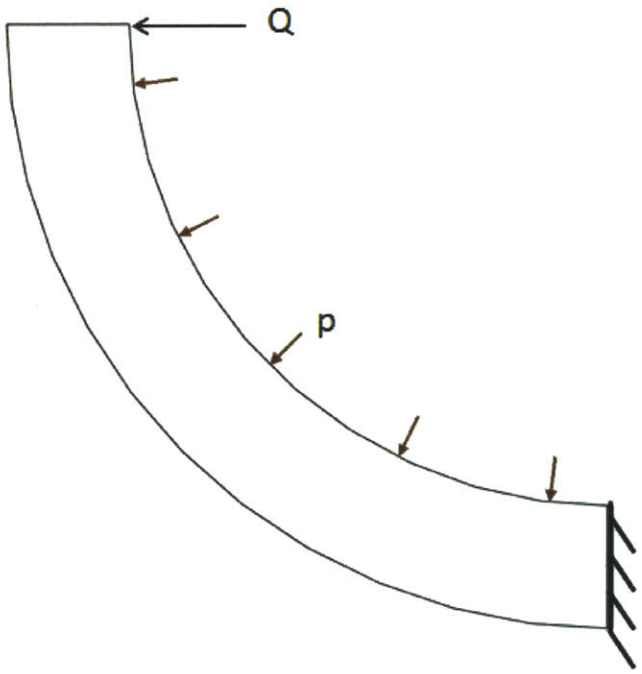

Figure D-1: Model of a half of the housing

Half of the housing is modeled as a curved cantilever beam of radius, R, with a constant line load, p, applied and one end fixed as seen in Figure D-1. A fictitious force, Q, is applied at $\theta = 0$ so deflection at that point can be found by Castigliano's method. The internal moment is calculated by examining a section of the beam shown

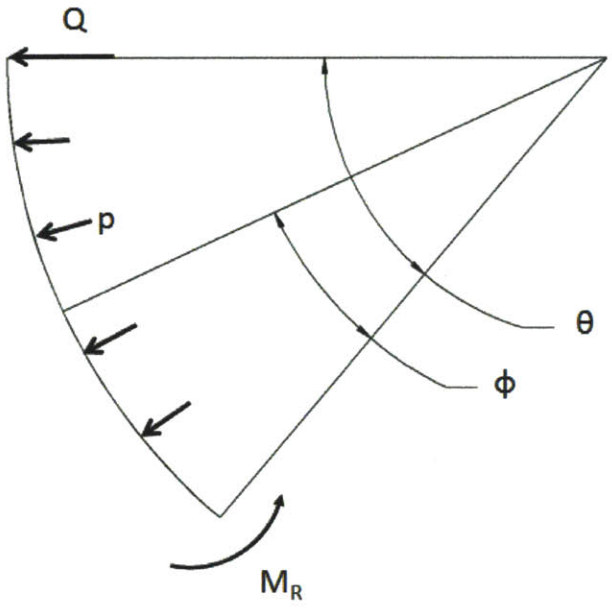

Figure D-2: The forces and moment on a section of the beam

in Figure D-2.

$$\begin{aligned}\sum M = 0 = M_R + \int_0^\theta pRsin\phi Rd\phi - QRsin\theta \\ M_R = -pR^2\left[-cos\phi\right]_0^\theta - QRsin\theta \\ = -pR^2(-cos\theta + 1) - QRsin\theta \\ = -pR^2(1 - cos\theta) - QRsin\theta \end{aligned} \tag{D.1}$$

Bending internal energy can then be calculated. Here the first term is evaluated

$$\begin{aligned} U &= \frac{1}{2EI}\int_0^{\pi/2} M_R^2 Rd\theta \\ &= \frac{1}{2EI}\int_0^{\pi/2} [-pR^2(1 - cos\theta) - QRsin\theta]^2 Rd\theta \\ &= \frac{R}{2EI}\int_0^{\pi/2} [p^2R^4(1 - cos\theta)^2 + 2pQR^3(1 - cos\theta)sin\theta + Q^2R^2sin^2\theta]d\theta \end{aligned} \tag{D.2}$$

To keep this derivation in a readable format, each term in the integral of (D.2) will

be evaluated separately. Here the first term is evaluated.

$$\begin{aligned}
&\int_0^{\pi/2} p^2R^4(1-cos\theta)^2 d\theta \\
=&p^2R^4 \int_0^{\pi/2} \left[1-2cos\theta+cos^2\theta\right] d\theta \\
=&p^2R^4 \left[\theta-2sin\theta+\frac{\theta}{2}+\frac{sin2\theta}{4}\right]_0^{\pi/2} \\
=&p^2R^4 \left[\frac{\pi}{2}-2+\frac{\pi/2}{2}\right] \\
=&p^2R^4 \left[\frac{\pi}{2}-2+\frac{\pi}{4}\right] \\
=&p^2R^4 \left[\frac{3\pi}{4}-2\right]
\end{aligned} \tag{D.3}$$

Now the second term in (D.2) is evaluated.

$$\begin{aligned}
&\int_0^{\pi/2} 2pQR^3(1-cos\theta)sin\theta d\theta \\
=&2pQR^3 \int_0^{\pi/2} \left[sin\theta-sin\theta cos\theta\right] d\theta \\
=&2pQR^3 \left[-cos\theta-\frac{1}{2}cos^2\theta\right]_0^{\pi/2} \\
=&2pQR^3 \left[\left(-cos\frac{\pi}{2}-\frac{1}{2}cos^2\frac{\pi}{2}\right)-\left(-cos0-\frac{1}{2}cos^20\right)\right] \\
=&2pQR^3 \left[-(-1-\frac{1}{2}(1)^2)\right] \\
=&2pQR^3\frac{3}{2} \\
=&3pQR^3
\end{aligned} \tag{D.4}$$

Finally, the second term in (D.2) is evaluated.

$$\begin{aligned}
&\int_0^{\pi/2} Q^2R^2 sin^2\theta d\theta \\
=&Q^2R^2\left[\frac{\theta}{2}-\frac{sin2\theta}{4}\right]_0^{\pi/2} \\
=&Q^2R^2\left[\left(\frac{\pi/2}{2}-\frac{sin\pi}{4}\right)-\left(\frac{0}{2}-\frac{sin0}{4}\right)\right]_0^{\pi/2} \\
=&\frac{\pi Q^2R^2}{4}
\end{aligned} \tag{D.5}$$

Combining (D.2), (D.3), (D.4), and (D.5) yields the final expression for internal bending energy.

$$U=\frac{R}{2EI}\left[p^2R^4\left(\frac{3\pi}{4}-2\right)+3pQR^3+\frac{\pi Q^2R^2}{4}\right] \tag{D.6}$$

Applying Castigliano's method yields the following.

$$\frac{\partial U}{\partial Q}=\frac{R}{2EI}\left[3pR^3+\frac{\pi QR^2}{2}\right] \tag{D.7}$$

The fictitious force, Q, is set to zero to find the expression for deflection.

$$\left.\frac{\partial U}{\partial Q}\right|_{Q=0}=\delta=\frac{3pR^4}{2EI} \tag{D.8}$$

The line load is related the the fluid pressure by multiplying the pressure by the depth into the page.

$$p=Pb \tag{D.9}$$

The section is a rectangle so the moment of inertia is calculated as follows.

$$I=\frac{1}{12}bh^3 \tag{D.10}$$

Combining (D.8), (D.9), and (D.10) yields the final expression for the deflection.

$$\begin{aligned}\delta &= \frac{3PbR^4}{2E\left(\frac{1}{12}bh^3\right)} \\ &= \frac{18PR^4}{Eh^3}\end{aligned} \tag{D.11}$$

The following values are used to calculate a rough estimate of the housing deflection.

- R = 0.05m
- h = 0.0127m
- P = 20psi = 137.986kPa
- E = 70GPA

Inputing these values into (D.11) yields the following.

$$\begin{aligned}\delta &= \frac{18(137,895Pa)(0.05m)^4}{(70X10^9Pa)(0.0127m)^3} \\ &= 0.108mm \\ &= 0.0043in\end{aligned} \tag{D.12}$$

This analysis is a rough estimate. The housing used for testing is a trough machined into a square block, so the moment of inertia is not contant. Also the fluid pressure is not constant inside the bearing. This estimate is a worst case scenario and points to the need for further investigation.

Bibliography

[1] L. D. Girard, *Hydraulique applique : nouveau systme de locomotion sur les chemins de fer.* Paris: Bachelier, 1852.

[2] F. W. Hoffer, "Automatic fluid pressure balancing system," U.S. Patent 2,449,297, Sept. 14, 1948.

[3] K. Wasson and A. Slocum, "Integrated shaft self-compensating hydrostatic bearing," U.S. Patent 5,700,092, Dec. 23, 1997.

[4] M. S. Kotilainen and A. H. Slocum, "Manufacturing of cast monolithic hydrostatic journal bearings," *Precision Engineering*, vol. 25, no. 3, pp. 235–244, June 2001.

[5] M. S. Kotilainen, "Design and manufacturing of modular self-compensating hydrostatic journal bearings," Ph.D. dissertation, Massachusetts Institute of Technology, Cambridge, 2000.

[6] K. L. Wasson, "Hydrostatic machine tool spindles," Ph.D. dissertation, Massachusetts Institute of Technology, Cambridge, 1996.

[7] W. B. Rowe, *Hydrostatic and Hybrid Bearing Design.* London: Butterworths, 1983.

[8] *Hydrodynamic plain journal bearings designed for operation under steady state conditions*, DIN Std. 31 652, 1983.

[9] A. Harnoy, *Bearing Design in Machinery : Engineering Tribology and Lubrication.* New York: Marcel Dekker, 2003.